

# In situ measurements of desert dust particles above the western Mediterranean Sea with the balloon-borne Light Optical Aerosol Counter/sizer (LOAC) during the ChArMEx campaign of summer 2013

Jean-Baptiste Renard<sup>1</sup>, François Dulac<sup>2</sup>, Pierre Durand<sup>3</sup>, Quentin Bourgeois<sup>4</sup>, Cyrielle Denjean<sup>5,b</sup>, Damien Vignelles<sup>1</sup>, Benoit Couté<sup>1</sup>, Matthieu Jeannot<sup>1,a</sup>, Nicolas Verdier<sup>5</sup>, Marc Mallet<sup>3,b</sup>

<sup>1</sup>Laboratoire de Physique et Chimie de l'Environnement et de l'Espace (LPC2E), UMR CNRS-Université d'Orléans, 3A avenue de la recherche scientifique, Orléans, France

<sup>2</sup>Laboratoire des Sciences du Climat et de l'Environnement (LSCE), UMR CEA-CNRS-UVSQ, IPSL, Université Paris-Saclay, CEA Saclay 701, Gif-sur-Yvette, France

<sup>3</sup>Laboratoire d'Aérodologie, Université de Toulouse, CNRS, UT3, Toulouse, France

<sup>4</sup>Department of Meteorology and Bolin Centre for Climate Research, Stockholm University, Stockholm, Sweden

<sup>6</sup>Centre National d'Etudes Spatiales (CNES), 18 Avenue Edouard Belin, Toulouse, France

<sup>a</sup>now at MeteoModem company, Chemin du Moulin, Ury, France

<sup>b</sup>now at Centre National de Recherches Météorologiques (CNRM), UMR Météo-France-CNRS, OMP, Météo-France, Toulouse, France

**Abstract.** Mineral dust from arid areas is a major component of the global aerosol and has strong interactions with climate and biogeochemistry. As part of the Chemistry-Aerosol Mediterranean Experiment (ChArMEx) to investigate atmospheric chemistry and its impacts in the Mediterranean region, an intensive field campaign was performed from mid-June to early August 2013 in the western basin including in situ balloon-borne aerosol measurements with the Light Optical Aerosol Counter (LOAC). LOAC is a counter/sizer that provides the aerosol concentrations in 19 size classes between 0.2 and 100  $\mu\text{m}$ , and an indication of the nature of the particles based on dual angle scattering measurements. A total of 27 LOAC flights were conducted mainly from Minorca Island (Balearic Islands, Spain) but also from Ile du Levant off Hyères city (SE France) under 17 Light Dilatable Balloons (meteorological sounding balloons) and 10 Boundary Layer Pressurized Balloons (quasi-Lagrangian balloons). The purpose was to document the vertical extent of the plume and the time-evolution of the concentrations at constant altitude (air density) by in situ observations. LOAC measurements are in agreement with ground-based measurements (lidar, photometer), aircraft measurements (counters), and satellite measurements (CALIOP) in case of fair spatial and temporal coincidences. LOAC has often detected 3 modes in the dust particle volume size distributions fitted by lognormal laws at roughly 0.2, 4 and 30  $\mu\text{m}$  in modal diameter. Thanks to the high sensitivity of LOAC, particles larger than 40  $\mu\text{m}$  were observed, with concentrations up to about  $10^{-4} \text{ cm}^{-3}$ . Such large particles were lifted several days before and their persistence after transport over long distances is in conflict with calculations of dust sedimentation. We did not observe any significant evolution of the size distribution during the transport from quasi-Lagrangian flights, even for the longest ones ( $\sim 1$  day). Finally, the presence of charged particles is inferred from the LOAC measurements and we speculate that electrical forces might counteract gravitational settling of the coarse particles.

## 1. Introduction

Mineral dust from arid and semi-arid areas is a major component of the global aerosol and has long been recognized to have strong interactions with climate and biogeochemistry (e.g., Buat-Ménard and Chesselet, 1979; Martin et al., 1991; Swap et al., 1992; Duce, 1995; Alpert et al., 1998; Mahowald et al., 2009; Maher et al., 2010; Liu et al., 2011; Mahowald et al., 2011; Chooari et al.,

52 2014; Li et al., 2016). Desert dust aerosol is of particular interest in the Mediterranean region where  
53 it is frequently observed in high concentrations in the troposphere, being a major component of  
54 surface PM<sub>10</sub> (Pey et al., 2013; Rea et al., 2015), aerosol optical depth (Moulin et al., 1998; Gkikas et  
55 al., 2013; Nabat et al., 2013), atmospheric deposition (Pye, 1992; Vincent et al., 2016), affecting the  
56 regional air quality (Querol et al., 2009), atmospheric thermodynamics (e.g. Alpert et al., 1998;  
57 Chaboureau et al., 2011), radiative budget and climate (e.g., Nabat et al., 2012, 2015a, 2015b),  
58 precipitation chemistry (Chester et al., 1996; Loÿe-Pilot et al., 1986; Avila and Rodà, 2002), soil  
59 formation (Nihlén et al., 1995), and biogeochemistry of forest ecosystems (Avila and Peñuelas, 1999),  
60 oligotrophic lakes (Morales-Baquero et al., 2006; Reche et al., 2009) and marine surface waters  
61 (Guerzoni et al., 1999; Herut et al., 1999; Guieu et al., 2014).

62 Most studies to characterize airborne dust particles transported long-range were performed  
63 with satellite remote sensing and/or surface in-situ and remote sensing instruments (counters,  
64 particles samplers, lidars, photometers...). Some aircraft observations were also conducted in situ  
65 inside dust plumes, but they are expensive and scarce (e.g., Schmid et al., 2000; Dulac and Chazette,  
66 2003; Haywood et al., 2003; Reid et al., 2003a; Formenti et al., 2008; Weinzierl et al., 2009; Weinzierl  
67 et al., 2011; Chen et al., 2011; Denjean et al., 2016), were often limited to several  $\mu\text{m}$  in terms of the  
68 particle size range covered and did not explore the same dust plume along its transport. One of the  
69 incompletely resolved issues is the evolution of the dust particle size distribution during long-range  
70 transport (Ansmann et al., 2011). It has been reported that an upward velocity counteracts  
71 gravitational sedimentation across the western Mediterranean (Dulac et al., 1992a) and North  
72 tropical Atlantic (Maring et al., 2003). Suggested causes include solar heating of dust layers (Prospero  
73 and Carlson, 1981), upward synoptic air mass movements (Dulac et al., 1992a), and turbulence (Ryder  
74 et al., 2013).

75 There is some debate in the literature on the very-long distance transport of coarse soil dust  
76 particles ( $>10 \mu\text{m}$  in diameter). It has been shown that a coarse mode at about  $14 \mu\text{m}$  in diameter is  
77 produced by sandblasting of arid soils by saltating sand grains (Alfaro et al., 1998; Alfaro and Gomes,  
78 2001). Furthermore, d'Almeida and Schütz (1983) report that African dust storm conditions produce  
79 a dust particle volume size distribution extending up to several tens of  $\mu\text{m}$  with a highly variable  
80 'giant' mode around  $60 \mu\text{m}$  in diameter. The modified Stokes-Einstein law indicates that steady state  
81 gravitational settling velocities ( $V_g$ ) of particles in air are proportional to the squared particle  
82 diameter (Stokes, 1851). For a particle density of  $2.5 \text{ g cm}^{-3}$  typical of soil dust,  $V_g$  reaches  $1 \text{ cm s}^{-1}$   
83 between  $11$  and  $12 \mu\text{m}$  and  $10 \text{ cm s}^{-1}$  between  $36$  and  $37 \mu\text{m}$ , i.e.  $860$  and  $8600 \text{ m d}^{-1}$ , respectively  
84 (Foret et al., 2006). Those giant particles are therefore expected to fall and control the dust  
85 deposition flux within the first  $1000 \text{ km}$  of transport from their source (Schütz et al., 1981). Maring et  
86 al. (2003) indicate that all Saharan dust particles larger than  $12 \mu\text{m}$  in diameter are scavenged  
87 between Canary Islands and Puerto Rico. However, there are evidences of Aeolian dust transport and  
88 sedimentation of giant dust particles in the ocean up to  $10\,000 \text{ km}$  away from source regions in the  
89 tropical Atlantic (Prospero et al., 1970; Carder et al., 1986) and Pacific (e.g. Betzer et al., 1988;  
90 Middleton et al., 2001; Jeong et al., 2014). Airborne observations also confirmed that the coarsest  
91 particles ( $>20 \mu\text{m}$  in diameter) are far from completely depleted over the North Atlantic (McConnell  
92 et al., 2008; Weinzierl et al., 2011; Ryder et al., 2013). Therefore, we still need observations of dust  
93 particle properties evolution over an extensive particle size range during their long-range transport;  
94 thus, there was a need of a new strategy for multiplying in-situ measurements of the dust particle  
95 size distribution. This was done for the first time in this study during African dust transport events  
96 above the western Mediterranean, deploying optical particle counters both below sounding balloons  
97 that crossed vertically the dust plume, and aboard drifting balloons that remained at constant  
98 altitude for quasi-Lagrangian measurements within the atmospheric dust layer.

99 The Chemistry-Aerosol Mediterranean Experiment (ChArMEx; <http://charmex.lscce.ipsl.fr>) is  
100 an international research initiative to investigate atmospheric chemistry in the Mediterranean region  
101 and its impacts on air quality, marine biogeochemistry and the regional climate. Within the project, a  
102 large regional field campaign was performed from mid-June to early August 2013 with intensive  
103 airborne measurements including in situ balloon-borne aerosol (Mallet et al., 2016) and ozone

104 (Gheusi et al., 2016) measurements. The observations were conducted during the dry season over  
105 the western and central Mediterranean basins. During the first special observation period (SOP)  
106 entitled Aerosol Direct Radiative Forcing on the Mediterranean Climate (ChArMEx/ADRMED SOP-1A)  
107 from mid-June to early July, the focus was on aerosol-radiation measurements and their modelling  
108 (Mallet et al., 2016). During the second SOP entitled Secondary Aerosol Formation in the  
109 Mediterranean (ChArMEx/SAFMED SOP-1B) from mid-July to early August, the focus was on  
110 atmospheric chemistry (Zannoni et al., 2017).

111 The present paper focuses on balloon-borne measurements conducted over the western  
112 Mediterranean during desert dust episodes encountered during this summer campaign with the new  
113 Light Optical Aerosol Counter (LOAC), an optical particle counter/sizer (OPC). Renard et al. (2016a  
114 and b) present the LOAC instrument and preliminary results from some flights analysed here with  
115 more details. In the following, we first briefly summarize the instrument principle and performances  
116 and we describe the different sounding and drifting balloon flights performed in summer 2013  
117 (section 2). Results on the particle size-segregated dust concentration are then presented, first in  
118 terms of vertical distribution (section 3), and secondly in terms of temporal evolution at constant  
119 altitudes (section 4). We then discuss dust particle sedimentation aspects (section 5) and  
120 speculations about electrically charged dust particles (section 6), and finally conclude (section 7).

121  
122

## 123 **2. Experimental strategy**

124

### 125 **2.1 Balloons-borne instruments**

126

127 This study is based on the LOAC instrument (Figure 1), a light OPC described and characterized by  
128 Renard et al. (2016a). Briefly, the instrument provides aerosol particle concentration measurements  
129 within 19 size classes in the 0.2–100  $\mu\text{m}$  diameter size range, and an estimate of the typology of  
130 aerosols based on dual angle measurements. LOAC can be carried by all kinds of balloons (Renard et  
131 al., 2016b). The gondola weight, including the instrument, the batteries (alkaline or lithium) and the  
132 telemetry system, is of about 1.0 kg, for an electric consumption of 3 W. Aerosols are sucked in by a  
133 small pump in order to pass through a red laser diode beam. In general, the light scattered by the  
134 particles depends on both the size and refractive index of the particles. To separate these two  
135 parameters, LOAC uses an original concept described in Renard et al. (2016a). Measurements are  
136 performed at 2 scattering angles: the first one is close to forward scattering at around  $12^\circ$  where the  
137 light scattered (diffracted) by non-spherical particles is controlled by the size of the particles (Lurton  
138 et al., 2014); the second one is around  $60^\circ$ , where the scattered light is strongly dependent on the  
139 refractive index of the particles (e.g., Weiss-Wrana, 1983; Renard et al., 2010; Francis et al., 2011).  
140 The  $12^\circ$  channel is used to retrieve the size distribution independently of the nature of the particles,  
141 and the combination of the  $12^\circ$  and  $60^\circ$  channels is used to derive the “LOAC speciation index” that  
142 informs on the typology or dominant nature of aerosol particles in each size range, based on a  
143 laboratory calibration conducted with particles of well-known nature. Figure 2 presents the reference  
144 “speciation zones” obtained in laboratory and an example of LOAC speciation index obtained during  
145 ambient air measurements inside a Saharan dust plume on 18 June above Minorca (Spain) at an  
146 altitude of 3.1 km.

147 As described by Renard et al. (2016a), the measurement uncertainty on the total aerosol  
148 concentration is  $\pm 20\%$  for concentration values greater than 1 particle per  $\text{cm}^3$  (for a 10-min  
149 integration time). In contrast, the uncertainty is up to about 60% for concentration values smaller  
150 than  $10^{-2}$  particle per  $\text{cm}^3$  for a 10-s integration time. In addition, the uncertainty in size calibration is  
151  $\pm 0.025 \mu\text{m}$  for particles smaller than  $0.6 \mu\text{m}$ , 5% for particles in the  $0.7\text{--}2 \mu\text{m}$  range, and 10% for  
152 particles larger than  $2 \mu\text{m}$ . Following coincidences, the measurement accuracy for submicronic  
153 particles could be reduced in a strongly turbid case when the concentration of particles larger than  $3$   
154  $\mu\text{m}$  exceeds a few particles per  $\text{cm}^3$ .

155 During the ChArMEx summer 2013 campaign, the LOAC gondolas were carried by two types  
156 of balloon: the Light Dilatable Balloon (LDB), a meteorological sounding balloon of about 1 kg, and  
157 the Boundary Layer Pressurized Balloon (BLPB), a drifting balloon of about 2.5 m in diameter.  
158 Pictures of the respective gondolas can be found in Renard et al. (2016b).

159 The LDB allows many flights from various places, and the gondola may generally be retrieved  
160 after landing (if not at sea). Measurements were conducted during the ascending phase of the  
161 balloon, at a speed of 3-6 m s<sup>-1</sup>. The inlet that collects aerosols was oriented toward the sky. The low  
162 flow rate (~1.7 L min<sup>-1</sup>) of the sampling pump yields sub-isokinetic sampling conditions that could  
163 tend to oversample large particles (Renard et al., 2016a). The highest altitude reached by LOAC was  
164 37 km, although in this study we will only consider the tropospheric part below 8 km in altitude (see  
165 Chane Ming et al. (2016) for an analysis of upper troposphere and stratosphere observations). The  
166 LOAC measurements, integrated every 10 s, are sent to ground in real-time by the on-board  
167 telemetry. To increase the measurement accuracy during the LDB ascent, the 10-s concentration  
168 values are averaged over a 1-min period, which provides a vertical resolution of about 300 m.

169 The BLPB, after its ascending phase, follows a near-Lagrangian trajectory, remaining in the  
170 same air mass during its trajectory in the lower atmosphere (Ethé et al. 2002; Gheusi et al., 2016;  
171 Doerenbecher et al., 2016). Its float altitude was prescribed before the flight (in the 400-3500 m  
172 range) by adjusting the balloon density with the appropriate mixture of air and helium. The altitude  
173 was chosen to fly within dust layers, based on a LDB flight and/or aerosol lidar measurements  
174 performed just before the launch. The horizontal speed of a drifting balloon relatively to ambient air  
175 is supposedly close to zero and the LOAC sampling the inlet was oriented horizontally, so that the  
176 particle sampling efficiency should be close to 100%. The integration time was chosen between 1 and  
177 20 min, due to the low telemetry rate for the downlink through the Iridium satellite communication  
178 system. The duration of the flights varied from several hours to more than one day. Also, LOAC was  
179 sometimes temporarily shut down after a session of measurements to save up on-board energy. For  
180 safety reasons, the authorized flight area was restricted to the sea (including islands).

181 The concentrations uncertainties are depending on the integration time. Higher is the  
182 integration time, more accurate are the measured concentrations; this is a strong constraint for the  
183 detection of the largest particles in low concentration. Typically, for concentration lower than 10<sup>-4</sup>  
184 particles cm<sup>-3</sup>, the uncertainties can be as high as 200% during a LDB flight, but down to 25% for the  
185 BLPB flights with an integration time of 20 min.

186  
187

## 188 **2.2 Other measurements**

189

190 The dust events were identified by near-real time (NRT) model and remote sensing products  
191 collected operationally by the ChArMEx Operation Centre web server (<http://choc.sedoo.fr>) where  
192 different quick-looks were made available. The main NRT remote sensing aerosol products were  
193 provided by 4-hourly observations from MSG/SEVIRI. The aerosol optical depth (AOD) at 550 nm  
194 (AOD<sub>550</sub>) product is based on Thieuleux et al. (2005).

195 In addition, we operated a calibrated ground-based CIMEL AERONET sun-photometer that  
196 provided AOD at 7 wavelengths from 340 to 1020 nm during daytime at the nearby station of Cap  
197 d'en Font on Minorca Island (39.826°N, 4.208°E; <http://aeronet.gsfc.nasa.gov>) where an aerosol and  
198 water vapour Raman lidar (WALI) with polarisation measurements was also in continuous operation  
199 (Chazette et al., 2016). The WALI lidar provides the vertical extent, the time-evolution and an  
200 estimate of the nature of the particles. The balloon launch site and the lidar and photometer station  
201 were distant by about 10 km.

202 The LOAC aerosol number concentration in the 0.2-100 µm range was converted to aerosol  
203 extinction using the Mie scattering theory, assuming spherical dust particles, to be compared to the  
204 lidar extinction data at 350 nm. The refractive index was set to 1.53-i0.0025, which corresponds to  
205 the mean value determined by Denjean et al. (2016) for the Saharan dust plume events documented  
206 during the summer 2013 ChArMEx campaign. This approach suffers from four approximations: i) all

207 counted particles are assumed to be mineral dust; ii) the contribution of the smallest particles is  
208 unknown, leading to some underestimation of the calculated aerosol extinctions; iii) the grains are  
209 considered as spherical while they are not; and iv) the refractive index of the grains is not always well  
210 known. In fact, the grains are irregular in shape and their refractive index can vary, depending on  
211 their composition and their origin, which potentially increases the uncertainty on our calculation on  
212 the aerosol extinction. Also, extinction calculations are highly sensitive to the size of the particles: the  
213 uncertainty in the LOAC particle size determination can produce a 50% uncertainty on the derived  
214 extinctions. The error bars on the LOAC-derived extinctions are calculated considering both  
215 concentration and size uncertainties. Weinzierl et al. (2009) report that accounting for the non-  
216 sphericity of dust particles might yield a small reduction of up to 5% in extinction computations  
217 based on the dust particle size distribution.

218 We used also the 532 nm aerosol extinction data in the troposphere obtained by the Cloud-  
219 Aerosol Lidar with Orthogonal Polarization (CALIOP on board the CALIPSO satellite) instrument,  
220 version 4.10 level-2, (e.g., Winker et al., 2009). The data have a horizontal resolution of 5 km and a  
221 vertical resolution of 60 m. Aerosol extinction values have a detection threshold of about  $0.01 \text{ km}^{-1}$ .  
222 The nature of aerosol particles and cloud droplets retrieved in CALIOP observations is given by the  
223 CALIOP vertical feature mask algorithm (Omar et al., 2009). To perform the comparison with CALIOP  
224 aerosol extinction data, the LOAC aerosol extinctions are calculated at 532 nm from the measured  
225 size distribution using the mineral dust refractive index as presented above

226 Finally, we use the aerosols measurements obtained during an ATR-42 aircraft flight close to  
227 Minorca. The instrumentation installed on board the aircraft is described in detail in Denjean et al.  
228 (2016). The aerosol size distribution was determined from an optical particle counter GRIMM 1.129  
229 (nominal size range  $0.25\text{-}32 \mu\text{m}$ ), an Ultra High Sensitivity Aerosol Spectrometer (UHSAS;  $0.04\text{-}1 \mu\text{m}$ )  
230 and a Forward Scattering Spectrometer Probe FSSP-300 ( $0.28\text{-}20 \mu\text{m}$ ). The UHSAS and FSSP are wing-  
231 mounted instruments, whereas the GRIMM installed inside the cabin received ambient air collected  
232 through the AVIRAD isokinetic inlet and tubing with a cut-off diameter of  $12 \mu\text{m}$  (Denjean et al.,  
233 2016).

234  
235

### 236 **2.3 Conditions of measurements**

237

238 Table 1 and Table 2 provide the conditions of measurements for LDB and BLPB flights  
239 performed during the ChArMEx campaign, respectively. Seventeen LDB flights and 10 BLPB flights  
240 were successfully performed during desert dust transport events, most of them launched from  
241 Minorca, the easternmost Balearic Island, Spain (latitude  $39.88^\circ\text{N}$ , longitude  $4.25^\circ\text{E}$ ) from 15 June to  
242 2 July, and a few from Ile du Levant, off Hyères city near the coast of south eastern France (latitude  
243  $43.02^\circ\text{N}$ , longitude  $6.46^\circ\text{E}$ ) from 27 July to 4 August (Figure 3). The confirmation of the occurrence of  
244 mineral dust plumes was possible from the LOAC-derived dominant typology of aerosol particles with  
245 the LOAC speciation index falling inside the “mineral zone” (Renard et al., 2016a,b).

246 In case of a Saharan dust event, the measurement strategy was to perform two LDB flights  
247 per day, and two simultaneous BLPB flights drifting at different altitudes within the dust plume (twin  
248 flights). The flight altitudes were chosen following real-time indications from the nearby lidar. This  
249 strategy was conducted during a relatively long dust event from 15 to 19 June, with 9 LDB flights and  
250 3 twin BLPB flights on June 15, 16, and 19. In terms of altitude, the twin flights were performed on 16  
251 June at the lower edge and in the middle of the dust layer, on 17 June both well inside the maximum  
252 concentration of the plume, and on 19 June at levels of minimum and maximum concentrations in  
253 the plume. The MODIS satellite observations indicate that the mean AOD was of about 0.25 during  
254 this period. The dust started to appear over the Alboran Sea on June 12. The daily average AOD  
255 derived from MSG/SEVIRI over the western Mediterranean basin from June 15 to 18 is mapped in  
256 Figure 4. It shows the arrival of the plume from the South-West with a low AOD over Minorca on  
257 June 15, its extension to the North and North-East on June 16 and 17 with a maximum extent of the  
258 plume over the basin on June 17, its reinforcement along a North-South axis on June 18 with the

259 largest AOD values around the Balearic Islands. On June 19 (not shown) Minorca was on the western  
260 edge of the plume that had shifted eastward.

261 Figure 5 shows times series of products from the WALI lidar from late June 15 to the end of  
262 June 17. The high extinction areas below 2.5 km until June 16, 13:00 are not or weakly depolarizing.  
263 Chazette et al. (2016; see their Figure 7) could infer from those data that the dominant aerosol was  
264 of marine nature around 500 m in altitude within the atmospheric boundary layer, dust above  
265 2.5 km, and pollution-related in between during the night of 15 to 16 June.

266 Five LDB flights were also conducted from Minorca Island during the 28 June-2 July period.  
267 Figure 6 shows maps of the daytime mean AOD over the western Mediterranean on 29 June and 2  
268 July. On 27-29 June, the Minorca region was impacted by turbid air masses arriving from the North-  
269 West (Chazette et al., 2016). Ancellet et al. (2016) identified long-range transport of forest fire smoke  
270 from different areas in North America (Canada and Colorado) and of African dust back from the  
271 western tropical Atlantic. Their Flexpart model simulations (Stohl et al., 2002) indicate that over  
272 Minorca, Canadian smoke aerosols dominated below 3 km on June 28 late afternoon, when dust  
273 dominated above 4 km and Colorado smoke aerosols were abundant above 5 km. Satellite-derived  
274 AOD shows that starting on June 29, a new dust plume from northwestern Africa with high AOD  
275 emerged from the Atlantic and Mediterranean coasts of Morocco. The plume extended a bit to the  
276 North and further East over the sea during the following days but remained confined to the  
277 southernmost part of the basin, with moderate AODs and some dust over Minorca on 2 July (AOD at  
278 550 nm up to 0.22, Chazette et al., 2016). A BLPB flight was conducted on 2 July; the mean MODIS  
279 AOD was of 0.15 during this period. Lidar data indicate that dust dominated between about 2 and 4.8  
280 km in altitude (Chazette et al., 2016). The aerosol in lower layers could not be typified.

281 Two other LDB flights were conducted from the Ile du Levant during a dust event on 27-28  
282 July. Twin BLPB flights were also performed in the upper edge of the plume. Finally, 2 LDB flights and  
283 one BLPB flight were conducted during a last dust event on 3-4 August. For those two events,  
284 daytime mean MSG-SEVIRI-derived AOD at 550 nm are up to about 0.30-0.35 off Levant Island  
285 (Figure 6).

286 From all those drifting balloon flights, it is possible to study the vertical extent of dust plumes  
287 and the temporal evolution of the dust particle size-segregated concentration at a given altitude  
288 during transport. In particular, LOAC data can be used to determine the concentration of large  
289 particles dominating the mass of desert dust transported and their deposition flux (e.g. Arimoto et  
290 al., 1985; Dulac et al., 1987, 1992a and b; Foret et al., 2006).

291  
292

### 293 **3. Vertical profiles and particle size distributions of the observed dust plumes**

294

295 The main desert dust event observed during the ChArMEx/ADRIMED campaign lasted five days from  
296 15 to 19 June as presented above (Figure 4). Figure 7 presents the vertical distribution of the 19 size  
297 class number concentrations, from the 9 LDB flights performed during that period. It shows that the  
298 dust plume was heterogeneously distributed in the free troposphere allowing for several local  
299 concentration maxima along the vertical and extended up to 7 km on the evening of 18 June. For  
300 comparison, Figure 8 presents measurements during a dust-free flight from Aire sur l'Adour, France  
301 (43.706°N, -0.251°E) on 14 August 2014, with no significant local concentration enhancement and  
302 the absence of large particles.

303 All these flights, including a BLPB flight on 19 June morning when LOAC performed  
304 measurements during the balloon ascent, were conducted concurrently to the nearby aerosol lidar  
305 measurements (Chazette et al., 2016). The time of the first 5 LDB flights are presented on the WALI  
306 lidar time-height cross-sections on June 16-17 with arrows marking (Figure 5). Figure 9 presents the  
307 tropospheric vertical profiles of the LOAC and WALI aerosol extinction observed during the 15-19  
308 June dust event over Minorca. Taking into account the uncertainties associated to the different  
309 instruments, the overall aerosol extinction values can be regarded as in the same order of  
310 magnitude, and even often in good agreement. LOAC and WALI have captured similar vertical

311 structures around half the time. The remaining discrepancies could be due to inaccurate size  
312 determination by LOAC, and to the distance between different observations of inhomogeneous dust  
313 plumes.

314 Three other dust events were documented with the LOAC instrument as illustrated by  
315 vertical profiles in Figure 10. The 28 June-2 July event was not intense in terms of aerosol  
316 concentration increase, while the 27-28 July and 3-4 August events were stronger. Similarly to the  
317 mid-June event, the dust plumes extended up to an altitude of 6 km and were not homogeneous in  
318 the vertical.

319 Good spatial and temporal coincidences occurred between LOAC measurements and CALIOP  
320 remote sensing measurements for two events: on 29-30 June above Minorca (Spain) and on 3 August  
321 above Ile du Levant (France). The LOAC measurements on 29-30 June were between 23:45 and 01:50  
322 UTC while the CALIOP measurements were at 01:56 UTC on 30 June. The LOAC measurements on 3  
323 August were between 11:15 UTC and 12:15 UTC while the CALIOP measurements were at 12:49 UTC  
324 Lidar WALI extinctions are also available for the 29 June at around 22:30 UTC.

325 Figure 11 presents the comparison between LOAC, CALIOP and WALI aerosol extinctions.  
326 During the 29-30 June night, the 3 instruments show that the plume extended from the ground to an  
327 altitude of 2.5 km. Although the general trend is in good agreement for the 3 instruments, local  
328 discrepancies are present in the vertical extinction profiles, possibly due to the temporal and spatial  
329 variability of the plume. LOAC seems to indicate a mixture of mineral dust and carbonaceous  
330 particles whereas CALIOP reports polluted continental/smoke particles (but the identification by  
331 CALIOP is difficult due to the weakness of the signal). On 30 June at mid-day, the plume had almost  
332 disappeared and the LOAC aerosol extinction values are below the detection threshold of CALIOP.

333 During the 3 August dust event, LOAC observations reveal that the plume extended from 2 to  
334 6.5 km. CALIOP captured all the dust plume in very good agreement with LOAC, and the two  
335 instruments identified the same nature of mineral dust particles. Another LOAC profile was obtained  
336 in the morning of 3 August at about 06:30 UTC, during a BLPB ascent up to its float altitude at 3 km  
337 (in blue in Figure 11. The two LOAC measurements are in very good agreement in the 2-3 km altitude  
338 range. Below 2 km, the two flight measurements show that the detected typologies are dominated  
339 by carbonaceous particles (likely anthropogenic aerosols). The strong temporal variability in particle  
340 concentrations below 2.2 km is therefore not related to the dust plume.

341 The ATR-42 aircraft flight was conducted close to Minorca (50 km apart) during dusty  
342 conditions in the morning of 16 June, at the same time of two LOAC balloon flights (LBD and BLBP).  
343 The aircraft probed the dust layer in the 2.5-4 km altitude range. Figure 12 presents the comparison  
344 of the size distributions measured by the 2 LOACs and the 3 aircraft counters at the maximum  
345 concentration level of the dust plume (2.5-4 km; see Figures 5 and 7). The integration from 2.5 to  
346 4 km of the LDB LOAC signal provides a better signal to noise ratio and a better sensitivity to the less  
347 numerous large particles (>15  $\mu\text{m}$ ) that are hardly detected with short integration times. Globally, all  
348 the instruments are in good agreement for the submicronic particles and for the coarse mode at 2-  
349 3  $\mu\text{m}$ ; the small discrepancies can be due to the difference in the respective measurement locations  
350 and to the different measurement methods of the various instruments, although they were all  
351 calibrated. The FSSP shows larger concentrations for particles larger than 2  $\mu\text{m}$  in diameter than  
352 other instruments (Figure 12). Reid et al. (2003b) discuss that the FSSP measurement principle tends  
353 to produce some oversizing of coarse particles and also shows particle concentrations as high as  
354 twice those measured by a Passive Cavity Aerosol Spectrometer Probe (PCASP) in their overlapping  
355 particle diameter range (1.5-3  $\mu\text{m}$ ). This could explain such a shift in our dataset. It is worth noting  
356 that the two LOACs, the FSSP and the GRIMM (despite the 12  $\mu\text{m}$  cut-off of its sampling inlet) all  
357 report particle concentrations larger than  $10^{-3} \text{ cm}^{-3}$  around 20  $\mu\text{m}$  in diameter. Both LOAC flights have  
358 detected similar concentrations of particles in the channels larger than 22  $\mu\text{m}$  in diameter. Although  
359 the GRIMM counter on board the ATR42 aircraft could sense particles up to 32  $\mu\text{m}$ , it did not report  
360 such larger grains, most probably because of the difficulty to collect and carry them up to the  
361 instrument inside the aircraft cabin.

362 In Figure 13, the LOAC-derived size distributions were converted to volume concentrations  
363 assuming spherical particles, using the mean volume diameter of each size class (Renard et al.,  
364 2016a), and integrated over the whole vertical. The LOAC volume size distribution is compared to  
365 that derived from the AERONET remote-sensing photometer during the 15-30 June 2013 dust events.  
366 On average, the AERONET and LOAC data are in good agreement regarding both the overall  
367 amplitude of the concentrations, and the position and the concentration of the coarse mode at  
368 about 3  $\mu\text{m}$  in radius. The better agreement is on the 16 June morning; the discrepancies for the  
369 other dates could be due to the local variability of the plume content since the LOAC and AERONET  
370 measurements are not conducted at the same time. Nevertheless, strong discrepancies sometimes  
371 occur for the smallest sizes (below 0.4  $\mu\text{m}$  in radius) and for the largest sizes (above 10  $\mu\text{m}$  in radius).  
372 The small-radius discrepancies could be due to local variability in the dust content, like on the 27  
373 June when AERONET retrieves a concentration increase centred on 0.25  $\mu\text{m}$  in radius, and to  
374 respective uncertainties of both methods. On the other end of the particle size range, AERONET  
375 retrieval is not very sensitive to the particles larger than 7  $\mu\text{m}$  in radius and the largest size class  
376 considered in the algorithm (15  $\mu\text{m}$  in radius) is limited to particles smaller than about 19.7  $\mu\text{m}$  in  
377 radius (Dubovik and King, 2000; Hashimoto et al., 2012). Thus, LOAC could have detected large  
378 particles that were not retrievable from AERONET observations.

379 Since the concentration of these large particles is low and subject to large uncertainties, the  
380 analysis of this mode from measurements during LBD flights is limited. Long duration measurements  
381 performed at constant altitude using the LOAC instrument on BLPB gondola with much longer  
382 integration time are better adapted to evaluate the concentration of these large particles (with an  
383 accuracy as good as 25%) and to discuss this third, giant size mode.

384  
385

#### 386 **4. Temporal evolution of the dust aerosol concentration and particle size distribution at** 387 **constant altitudes**

388

389 Figure 14 presents results from the BLPB flights performed inside dust plumes. In particular,  
390 the 27-28 June and the 2-3 July BLPB flights were the longest ones, with duration of about 1 day.  
391 Day-night transitions were thus encountered, leading to a decrease in float altitude during the night  
392 of more than 100 m due to the cooling of the balloon gas and associated loss in buoyancy, so that the  
393 night-time and daytime measurements were not conducted in exactly the same air mass.

394 The slow speed ascent of the 19 June and 3 August BLPBs allowed us to obtain two additional  
395 fine-resolution vertical profiles in the lower troposphere. The LOAC aerosol concentration values  
396 obtained during the BLPB ascent on 19 June are in good agreement with the LBD ascent  
397 measurements conducted at the same time (Figure 9, lower right panel). In particular, LOAC has well  
398 captured the vertical variation of the dust plume concentrations, with a local minimum at an altitude  
399 of 2 km.

400 During most of the flights, particles larger than 40  $\mu\text{m}$  in diameter (last LOAC channel) were  
401 detected. The concentration of these particles depends mainly on the intensity of the event, but the  
402 highest concentration was detected in the free troposphere on 19 June, with about  $10^{-4}$  particles per  
403  $\text{cm}^3$  at an altitude of 3.3 km. It can be noticed that concentrations of  $10^{-3}$  particles per  $\text{cm}^3$  were  
404 detected at ground at the same date, as shown in Figure 7.

405 The dust particle volume size distributions were computed by integrating data over more  
406 than a minute at a constant altitude. The mean diameter of the last channel was assumed to be 50  
407  $\mu\text{m}$ , although the size range is 40-100  $\mu\text{m}$ , because the concentrations strongly decrease with size  
408 and most of the particles thus have a diameter close to the lower limit of the size class. Those volume  
409 distributions were then fitted with a 3-mode log-normal model using a least-square procedure. The  
410 three-fitted volume modal diameters ( $D_m$ ) have been found at about 0.2, 4 and 30  $\mu\text{m}$  as illustrated  
411 in Figure 15. Note, however, that only the decreasing part of the first (small) mode is captured by  
412 LOAC and the corresponding modal diameter could therefore be misestimated. There is also some



413 uncertainty on the third (large) mode related to the assumed upper limit of the measurement size  
414 range and to the possible under-sampling of the upper tail of the size distribution; thus this mode  
415 value may be a lower limit.

416 Figure 16 shows the evolution of  $D_m$  for the three modes fitted from the 3 pairs of BPCL  
417 LOAC data obtained during the 15-19 June dust event. BLPB flights lasted between 6 and 11 hours.  
418 No significant temporal trend can be pointed out for  $D_m$ , meaning that the size distribution remains  
419 almost constant over hours. Thus, it seems that no significant sedimentation has been detected  
420 during the flights at quasi-constant altitude even for the very coarse mode at about 30  $\mu\text{m}$  in  
421 diameter.

422 Table 3 gives the values of  $D_m$  for the 3 modes at float altitude for the 6 BPCL flights in dust  
423 layers during the 16-19 June event; the average values are 0.26, 3.7 and 30.4  $\mu\text{m}$ , respectively.  
424 Values for the 3 modes are very comparable from one balloon to the other with a small variability of  
425 about 15%, likely not significant given the uncertainties of the fitting. The flights inside the other dust  
426 events confirm the presence of large particles in a giant mode at about 30  $\mu\text{m}$  in diameter.  
427 Nevertheless, some variations in aerosol concentrations often occurred. They are due to changes in  
428 the balloon altitude during the day-night transition for the 27-28 June and the 2-3 July flights, to a  
429 non-constant altitude for the 28 June flight, and to a slow ascent during the 3 July flight. These  
430 variations of concentration are thus probably related to vertical variations of the dust plume layer.  
431 Indeed, lidar profiles from Minorca show a strong vertical structuration of aerosol layers (Chazette et  
432 al., 2016) that could be associated with significant differences in aerosol composition, concentration  
433 and size distribution. Hamonou et al. (1999) first documented the multi-layered African dust  
434 transport over the Mediterranean basin with variable source regions of mineral dust particles found  
435 in different layers of the plume.

436 The presence of the third, very coarse mode with  $D_m$  of the order of 30  $\mu\text{m}$  may be related  
437 to the existence of a mode in desert dust aerosols: a value of the same order ( $D_m = 42.3 \mu\text{m}$ ) is  
438 assumed in the model of background desert dust aerosol of Jaenicke (1987). Observations of a very  
439 coarse mode are also reported by Weinzierl et al. (2009): particles larger than 20  $\mu\text{m}$  were detected  
440 in nine out ten cases of 49 pure dust layers observed in altitude over southern Morocco with wing-  
441 mounted airborne optical particle counters. In 20% of the cases, particle sizes equal or larger than 40  
442  $\mu\text{m}$  and up to 80  $\mu\text{m}$  were detected (with a detection limit of  $10^{-2} \text{ cm}^{-3}$ ). They report an average  
443 volume median diameter of the coarse mode of  $15.5 \pm 10.9 \mu\text{m}$  near dust source region and a  
444 maximum value larger than 60  $\mu\text{m}$  in a case of strong convection. Weinzierl et al. (2011) also report  
445 that particles more than 20  $\mu\text{m}$  in diameter (but  $< 30 \mu\text{m}$ ) are still found at concentrations  
446  $> 10^{-2} \text{ cm}^{-3}$  in 1/3 of 24 dust transport cases documented over the eastern tropical North Atlantic. The  
447 better sensitivity of LOAC may explain why we report more systematically a coarse mode of dust  
448 particles above 20  $\mu\text{m}$  in diameter. However, the persistence of such large particles, lifted several  
449 days ago, and their transport above the Mediterranean basin is not well understood given their large  
450 theoretical settling velocity.

451

452

## 453 5. Discussion related to dust sedimentation

454

455 According to the Stoke's approximation that equates the effective weight of spherical  
456 particles and the viscous resistance of the fluid through which it moves (Stokes, 1851), the  
457 gravitational settling velocity  $V_g$  of dust particles is proportional to the square of their diameter.  
458 Assuming a classical density value of  $2.5 \text{ g cm}^{-3}$  for spherical dust particles (Dulac et al., 1989; Zender  
459 et al., 2003; Linke et al., 2006),  $V_g$  is thus about 0.0076, 0.19, 0.76, 3.0, 6.8, and  $19 \text{ cm s}^{-1}$  for particles  
460 of 1, 5, 10, 20, 30 and 50  $\mu\text{m}$  in diameter, respectively, implying a downward transport ranging from  
461 about 6.6 to  $16 \text{ 400 m d}^{-1}$ . Particles larger than 12.3  $\mu\text{m}$  have a sedimentation velocity larger than  
462  $1 \text{ 000 m d}^{-1}$ . This is supposed to yield a quick segregation and a rapid evolution of the dust particle  
463 size distribution in the first days (and even hours) of transport after lifting from the dust source  
464 region (e.g., Schütz et al., 1981; see also Figure 1 in Foret et al., 2006). Dust-loaded air masses

465 transported northward from Africa above the marine atmospheric boundary layer in the western  
466 Mediterranean are known to be associated with warm fronts and to experience a significant upward  
467 synoptic movement (Prodi and Fea, 1979; Reiff et al., 1986). Dulac et al. (1992a and b) report that  
468 during a typical summer dust episode the turbid air mass ascending velocity was on average of the  
469 order of 1.5 to 1.8 cm s<sup>-1</sup> for 4 days, i.e. was more than compensating the average deposition velocity  
470 of the bimodal dust particle size distribution observed in Corsica during this event, with 2 modes at 2  
471 and 13 μm. This is not enough, however, to explain the relatively constant dust particle size  
472 distribution observed during BPCL flights: accounting for an average upward air mass vertical velocity  
473 of 1.5 cm s<sup>-1</sup> that would counteract gravitation, a 4-km thick dust layer should anyway lose by  
474 sedimentation all particles larger than 30 μm in about 1 day.

475 According to Slinn (1983; eq. 160), the flux-mean deposition velocity ( $\langle V_d \rangle$ ) of a lognormal  
476 distribution of particles of modal diameter  $Dm$  and geometric standard deviation  $\sigma_g$  can be derived  
477 from  $\langle V_d \rangle = V_d(Dm) \sigma_g^{2\ln(\sigma_g)}$ . Using this formula, we can derive that the 3-fitted dust particle size  
478 modes shown in Figure 15 have a respective gravitational settling velocity of about 0.0011, 0.50, and  
479 8.1 cm s<sup>-1</sup>, corresponding to a negligible downward transport by sedimentation of about 1 m d<sup>-1</sup> for  
480 the finest mode, but to 430 m d<sup>-1</sup> for the intermediate mode, and as much as 7 000 m d<sup>-1</sup> for the  
481 largest one. Figure 14 does not show any significant systematic evolution of the concentration of the  
482 different modes. New particles sedimenting from turbid layers above the balloon might compensate  
483 for the sedimentation of particles from the intermediate coarse mode with  $Dm$  of about 4 μm during  
484 our 1-d or less balloon flight times. However, we should definitely observe a significant decrease in  
485 the concentration and median size of the very coarse mode with  $Dm \approx 30$  μm. Figure 16 does not  
486 show any evidence of a decrease in the very coarse mode median diameter.

487  
488

## 489 **6. Indirect detection of possible charged particles**

490

491 Laboratory tests have shown that the LOAC photodiode and electronics are sensitive to  
492 electromagnetic fields, as those generated by radio telemetry, by strong atmospheric electric activity  
493 (e.g., during thunderstorms), and even by an electrical bay. In these cases, the electronic noise and  
494 the electronic offset both increase. The offset also increases with increasing ambient temperature.

495 LOAC performs measurements of the electronic noise and offset every 15 min when the light  
496 source is switched off (Renard et al., 2016a). During a typical LDB flight, the LOAC electronic offset  
497 slightly decreased with altitude due to the decreasing temperature encountered during the balloon  
498 ascent. In contrast, an offset increase coincident with the increase in dust particle concentration was  
499 detected for 5 flights when crossing a dust plume, as shown in Figure 17. Such an offset increase was  
500 never observed outside the plumes.

501 Laboratory tests have shown that indeed the LOAC electronics is very sensitive to  
502 electromagnetic fields, with an increase of the offset. These offset increases may be related to the  
503 presence of local strong electromagnetic fields inside the plume, although it is not possible to  
504 retrieve their strength with such kinds of measurements. It is known that the aerosol generation  
505 from both mineral dust powders (e.g., Johnston et al., 1987; Forsyth et al., 1998) and arid soils (e.g.  
506 Ette, 1971; Farrell et al., 2004; Sow et al., 2011) produces charged particles, and that electrical  
507 charges in sandstorms perturb telecommunication transmissions (e.g. Li et al., 2010 and references  
508 therein). The presence of electric field in dust aerosol layers was indeed proposed by Ulanowski et al.  
509 (2007) to explain the alignment of non-spherical particles and polarization effects in a dust plume  
510 over the Canary Islands. Nicoll et al. (2011) also report charged particles within Saharan dust layers  
511 with two balloon soundings performed above Cape Verde Islands.

512 We suggest that electric forces within the dust layers could contribute maintaining in  
513 levitation coarse particles that would otherwise expected to sediment down. Future balloon  
514 campaigns with LOAC measurement in parallel with an adequate instrument retrieving accurately the  
515 atmospheric electric field could consolidate these previous studies. This looks as an important

516 perspective to consider since the local electric field in dust plume might be at least partly responsible  
517 for the non-sedimentation of large particles resulting in much longer transport than expected.  
518

519

## 520 **7. Conclusions**

521

522 The in-situ LOAC balloon-borne measurements above the Mediterranean basin in summer 2013 have  
523 allowed us to document both the vertical extent of the dust plumes and, for the first time to our  
524 knowledge, the time-evolution of dust concentrations from several hours to one day in a quasi-  
525 Lagrangian way at constant altitude. Whenever possible, LOAC observations were compared to the  
526 measurements done by other platforms, like the ATR-42 aircraft which embarked various aerosol  
527 counters, and a backscattering lidar located close to the balloon launching area. Given the limits and  
528 uncertainties associated with each measurement system, the agreement was satisfactory, which  
529 gave us confidence in the LOAC aerosol distributions. LOAC has often detected the presence of  
530 particles larger than 40  $\mu\text{m}$ , with concentrations up to  $10^{-4}$  particles per  $\text{cm}^3$ , and the fitting of  
531 volume size distribution ended up in a coarse mode at 3-4  $\mu\text{m}$  in diameter and a giant mode at about  
532 30  $\mu\text{m}$ . Such large particles should have been lifted several days before, and at least 1 000 km far  
533 from our measurements. Their transport over such long distances, not expected from calculations of  
534 dust particle sedimentation, is yet not well understood. Indeed, the gravitational settling velocity of  
535 dust particles between 12 and 40  $\mu\text{m}$  in diameter spans from almost 1 to more than 10 km per day.  
536 An indirect evidence of the presence of charged particles has been derived from the LOAC  
537 measurements and we therefore hypothesize that electric forces within the dust plume might limit  
538 the sedimentation of the coarse dust fraction.

539 ChArMEx was a unique experiment involving a large set of ground-based and airborne  
540 instruments. Since 2014, regular LDBs with LOAC are launched twice a month from Aire-sur-l'Adour  
541 (South-West of France, 43.71°N, 0.25°W) to monitor the aerosol content from the troposphere to the  
542 stratosphere. Dust events were already occasionally detected; they will be used to document other  
543 dust events than those of summer 2013 with the same instrument, and to confirm the presence of  
544 both the large particles and the charged particles thanks to new developments of the instrumental  
545 payload.  
546

547

548 **Acknowledgements.** The LOAC development project was funded by the French National Research  
549 Agency's ANR ECOTECH. The balloon flights of the MISTRALS/ChArMEx campaign were funded and  
550 performed by the French Space Agency CNES. The LOAC instruments are built by Environnement-SA  
551 company; the balloon-borne gondolas are provided by MeteoModem company and by CNES for  
552 sounding and drifting balloons, respectively. The numerous LOAC instruments used during the  
553 campaign and the scientific and technical staff missions were funded with the support of CNES, INSU-  
554 CNRS and ADEME. Airborne data was obtained using the ATR-42 Atmospheric Research Aircraft  
555 managed by Safire, which is a joint facility of CNRS, Météo-France and CNES. The SAFIRE team is  
556 acknowledged for the aircraft operation. The French VOLTAIRE-LOAC Labex (Laboratoire d'Excellence  
557 ANR-10-LABX-100-01) also provided a couple of LOAC instruments. The PHOTONS  
558 (<http://loaphotons.univ-lille1.fr/>) and AERONET (<https://aeronet.gsfc.nasa.gov/>) teams are  
559 acknowledged for our sun-photometer calibration and data processing, respectively. P. Chazette and  
560 J. Totems are acknowledged for lidar data from Minorca, and P. Formenti for her contribution to  
561 airborne data acquisition and reference suggestions. We also thank O. Dubovik for his comments on  
562 the AERONET inversion limitation for large particles. ChArMEx LOAC balloon and other  
563 measurements are available on the ChArMEx database (<http://mistrals.sedoo.fr/ChArMEx/>). Finally,  
564 CALIOP data have been retrieved through the ICARE Data Services and Center  
565 (<http://www.icare.univ-lille1.fr>).

566

567

568 **References**

569

570 Alfaro, S. C., and Gomes, L.: Modeling mineral aerosol production by wind erosion: Emission  
571 intensities and aerosol size distributions in source areas, *J. Geophys. Res.*, 106, 18075–18084,  
572 doi:10.1029/2000JD900339, 2001.

573 Alfaro, S. C., Gaudichet, A., Gomes, L., and Maillé, M.: Mineral aerosol production by wind erosion:  
574 Aerosol particle sizes and binding energies, *Geophys. Res. Lett.*, 25, 991-994,  
575 doi:10.1029/98GL00502, 1998.

576 Alpert, P., Kaufman, Y. J., Shay-El, Y., Tanré, D., da Silva, A., Schubert, S., and Joseph, J. H.:  
577 Quantification of dust-forced heating of the lower troposphere, *Nature*, 395, 367-370,  
578 doi:10.1038/26456, 1998.

579 Ancellet, G., Pelon, J., Totems, J., Chazette, P., Bazureau, A., Sicard, M., Di Iorio, T., Dulac, F., and  
580 Mallet, M.: Long-range transport and mixing of aerosol sources during the 2013 North American  
581 biomass burning episode: analysis of multiple lidar observations in the western Mediterranean  
582 basin, *Atmos. Chem. Phys.*, 16, 4725-4742, doi:10.5194/acp-16-4725-2016, 2016.

583 Ansmann, A., Petzold, A., Kandler, K., Tegen, I., Wendisch, M., Müller, D., Weinzierl, B., Müller, T. and  
584 Heintzenberg, J.: Saharan Mineral Dust Experiments SAMUM-1 and SAMUM-2: what have we  
585 learned?, *Tellus B*, 63: 403–429. doi:10.1111/j.1600-0889.2011.00555.x, 2011.

586 Arimoto, R., Duce, R. A., Ray, B. J., and Unni, C. K.: Atmospheric trace elements at Enewetak Atoll: 2.  
587 Transport to the ocean by wet and dry deposition, *J. Geophys. Res.*, 90, 2391–2408,  
588 doi:10.1029/JD090iD01p02391, 1985.

589 Avila, A. and Peñuelas, J.: Increasing frequency of Saharan rains over northeastern Spain and its  
590 ecological consequences, *Sci. Total Environ.*, 228, 153-156, doi:10.1016/S0048-9697(99)00041-8,  
591 1999.

592 Avila, A. and Rodà, F.: Assessing decadal changes in rainwater alkalinity at a rural Mediterranean site  
593 in the Montseny Mountains (NE Spain), *Atmos. Environ.*, 36, 2881-2890, doi:10.1016/S1352-  
594 2310(02)00098-5, 2002.

595 Betzer, P. R., Carder, K. L., Duce, R. A., Merrill, J. T., Tindale, N. W., Uematsu, M., Costello, D. K.,  
596 Young, R. W., Feely, R. A., Breland, J. A., Bernstein, R. E., and Greco, A. M.: Long-range transport of  
597 giant mineral aerosol particles, *Nature*, 336, 568-571, doi:10.1038/336568a0, 1988.

598 Buat-Ménard, P. and Chesselet, R.: Variable influence of the atmospheric flux on the trace metal  
599 chemistry of oceanic suspended matter, *Earth Planet. Sci. Lett.*, 42, 399-411, doi:10.1016/0012-  
600 821X(79)90049-9, 1979.

601 Carder, K. L., Stewards, R. G., Betzer, P. R., Johnson, D. L., and Prospero, J. M.: Dynamics and  
602 composition of particles from an Aeolian input event to the Sargasso Sea, *J. Geophys. Res.*, 91,  
603 1055-1066, doi:10.1029/JD091iD01p01055, 1986.

604 Chaboureaud, J.-P., Richard, E., Pinty, J.-P., Flamant, C., Di Girolamo, P., Kiemle, C., Behrendt, A.,  
605 Chepfer, H., Chiriaco, M., and Wulfmeyer, V.: Long-range transport of Saharan dust and its  
606 radiative impact on precipitation forecast: a case study during the Convective and Orographically-  
607 induced Precipitation Study (COPS), *Q. J. R. Meteorol. Soc.*, 137, 236–251, doi:10.1002/qj.719,  
608 2011.

609 Chane Ming, F., Vignelles, D., Jegou, F., Berthet, G., Renard, J.-B., Gheusi, F., and Kuleshov, Y.:  
610 Gravity-wave effects on tracer gases and stratospheric aerosol concentrations during the 2013  
611 ChArMEx campaign, *Atmos. Chem. Phys.*, 16, 8023-8042, doi:10.5194/acp-16-8023-2016, 2016.

612 Chazette, P., Totems, J., Ancellet, G., Pelon, J., and Sicard, M.: Temporal consistency of lidar  
613 observations during aerosol transport events in the framework of the ChArMEx/ADRIMED  
614 campaign at Minorca in June 2013, *Atmos. Chem. Phys.*, 16, 2863-2875, doi:10.5194/acp-16-2863-  
615 2016, 2016.

616 Chen, G., Ziemba, L. D., Chu, D. A., Thornhill, K. L., Schuster, G. L., Winstead, E. L., Diskin, G. S.,  
617 Ferrare, R. A., Burton, S. P., Ismail, S., Kooi, S. A., Omar, A. H., Slusher, D. L., Kleb, M. M., Reid, J. S.,  
618 Twohy, C. H., Zhang, H., and Anderson, B. E.: Observations of Saharan dust microphysical and

619 optical properties from the Eastern Atlantic during NAMMA airborne field campaign, *Atmos.*  
620 *Chem. Phys.*, 11, 723-740, <https://doi.org/10.5194/acp-11-723-2011>, 2011.

621 Chester, R., Nimmo, M., and Keyse, S.: The influence of Saharan and Middle Eastern desert-derived  
622 dust on the trace metal composition of Mediterranean aerosols and rainwater, in *The Impact of*  
623 *Desert Dust Across the Mediterranean*, Guerzoni, S., and Chester, R., Eds., Kluwer, 253-273, 1996.

624 Choobari O. A., Zawar-Reza, P., and Sturman, A.: The global distribution of mineral dust and its  
625 impacts on the climate system: A review, *Atmso. Res.*, 138, 152-165,  
626 doi:10.1016/j.atmosres.2013.11.007, 2014.

627 D'Almeida, G. A. and Schütz, L.: Number, mass and volume distribution of mineral aerosol and soils of  
628 the Sahara, *J. Climate Appl. Meteor.*, 22, 233-243, doi:10.1175/1520-  
629 0450(1983)022<0233:NMAVDO>2.0.CO;2, 1983.

630 Denjean, C., Cassola, F., Mazzino, A., Triquet, S., Chevaillier, S., Grand, N., Bourrienne, T., Momboisse,  
631 G., Sellegri, K., Schwarzenbock, A., Freney, E., Mallet, M., and Formenti, P.: Size distribution and  
632 optical properties of mineral dust aerosols transported in the western Mediterranean, *Atmos.*  
633 *Chem. Phys.*, 16, 1081–1104, doi:10.5194/acp-16-1081-2016, 2016.

634 Doerenbecher, A., C. Basdevant, Ph. Drobinski, P. Durand, C. Fesquet, F. Bernard, Ph. Cocquerez, N.  
635 Verdier and A. Vargas.: Low atmosphere drifting balloons: platforms for environment monitoring  
636 and forecast improvement, *Bull. Amer. Meteor. Soc.*, 97, 1583–1599, doi:10.1175/BAMS-D-14-  
637 00182.1.

638 Dubovik, O. and King, M. D.: A flexible inversion algorithm for retrieval of aerosol optical properties  
639 from Sun and sky radiance measurements, *J. Geophys. Res.*, 105, 20673-20696,  
640 doi:10.1029/2000JD900282, 2000.

641 Duce, R. A.: Sources, distributions, and fluxes of mineral aerosols and their relationship to climate, in  
642 *Aerosol Forcing of Climate*, Charlson, R. J., and Heintzenberg, J., Eds., Wiley, 43-72, 1995.

643 Dulac, F. and Chazette, P.: Airborne study of a multi-layer aerosol structure in the eastern  
644 Mediterranean observed with the airborne polarized lidar ALEX during a STAAARTE campaign (7  
645 June 1997), *Atmos. Chem. Phys.*, 3, 1817-1831, doi:10.5194/acp-3-1817-2003, 2003.

646 Dulac, F., Buat-Ménard, P., Arnold, M., Ezat, U., and Martin, D: Atmospheric input of trace metals to  
647 the western Mediterranean Sea: 1. Factors controlling the variability of atmospheric  
648 concentrations, *J. Geophys. Res.*, 92, 8437-8453, doi:10.1029/JD092iD07p08437, 1987.

649 Dulac, F., Buat-Ménard, P., Ezat, U., Melki, S., and Bergametti, G. : Atmospheric input of trace metals  
650 to the western Mediterranean: uncertainties in modelling dry deposition from cascade impactor  
651 data, *Tellus*, 41B, 362-378, doi:10.1111/j.1600-0889.1989.tb00315.x, 1989.

652 Dulac, F., Bergametti, G., Losno, R., Remoudaki, E., Gomes, L., Ezat, U., and Buat-Ménard, P.: Dry  
653 deposition of mineral aerosol particles: significance of the large size fraction, in *Precipitation*  
654 *Scavenging and Atmosphere-Surface Exchange*, Schwartz, S. E., and Slinn W. G. N. Eds., 2, 841-  
655 854, Hemisphere, Richland, WA, 1992a.

656 Dulac, F. Tanré, D., Bergametti, G., Buat-Ménard, P., Desbois, M., and Sutton, D. : Assessment of the  
657 African airborne dust mass over the western Mediterranean Sea using Meteosat data, *J. Geophys.*  
658 *Res.*, 97, 2489-2506, doi:10.1029/91JD02427, 1992b.

659 Ethé, C., Basdevant, C., Sadourny, R., Appu, K. S., Harenduprakash, L., Sarode, P. R., and Viswanathan,  
660 G.: Air mass motion, temperature and humidity over the Arabian Sea and western Indian Ocean  
661 during the INDOEX intensive phase, as obtained from a set of superpressure drifting balloons, *J.*  
662 *Geophys. Res.*, 107, 8023, doi:10.1029/2001JD001120, 2002.

663 Ette, A. I. I.: The effect of the Harmattan dust on atmospheric electric parameters, *J. Atmos. Terr.*  
664 *Phys.*, 33, 295-300, doi:10.1016/0021-9169(71)90208-X, 1971.

665 Farrell, W. M., Smith, P. H., Delory, G. T., Hillard, G. B., Marshall, J. R., Catling, D., Hecht, M., Tratt, D.  
666 M., Renno, N., Desch, M. D., Cummer, S. A., Houser, J. G., and Johnson, B.: Electric and magnetic  
667 signatures of dust devils from the 2000–2001 MATADOR desert tests, *J. Geophys. Res.*, 109,  
668 E03004, doi:10.1029/2003JE002088, 2004.

669 Foret, G., Bergametti, G., Dulac, F. and Menut, L.: An optimized particle size bin scheme for modeling  
670 mineral dust aerosol, *J. Geophys. Res.*, 111, D17310, doi:10.1029/2005JD006797, 2006.

671 Formenti, P., Rajot, J. L., Desboeufs, K., Caquineau, S., Chevaillier, S., Nava, S., Gaudichet, A., Journet,  
672 E., Triquet, S., Alfaro, S., Chiari, M., Haywood, J., Coe, H., and Highwood, E.: Regional variability of  
673 the composition of mineral dust from western Africa: Results from the AMMA SOP0/DABEX and  
674 DODO field campaigns, *J. Geophys. Res.*, 113, D00C13, doi:10.1029/2008JD009903, 2008.

675 Forsyth, B., Liu, B. Y. H., and Romay, F. J.: Particle charge distribution measurements for commonly  
676 generated laboratory aerosol, *Aerosol Sci. Technol.*, 28, 489-501,  
677 doi:10.1080/02786829808965540, 1998.

678 Francis, M., Renard, J.-B., Hadamcik, E., Couté, B., Gaubicher, B., and Jeannot, M.: New studies on  
679 scattering properties of different kinds of soot, *J. Quant. Spectr. Rad. Transf.*, 112, 1766-1775,  
680 doi:10.1016/j.jqsrt.2011.01.009, 2011.

681 Gheusi, F., Durand, P., Verdier, N., Dulac, F., Attié, J.-L., Commun, P., Barret, B., Basdevant, C., Clenet,  
682 A., Derrien, S., Doerenbecher, A., El Amraoui, L., Fontaine, A., Hache, E., Jambert, C., Jaumouillé,  
683 E., Meyerfeld, Y., Roblou, L., and Tocquer, F.: Adapted ECC ozonesonde for long-duration flights  
684 aboard boundary-layer pressurised balloons, *Atmos. Meas. Tech.*, 9, 5811-5832, doi:10.5194/amt-  
685 9-5811-2016, 2016.

686 Guerzoni, S., Chester, R., Dulac, F., Herut, B., Loÿe-Pilot, M.-D., Measures, C., Migon, C., Molinaroli, E.,  
687 Moulin, C., Rossini, P., Saydam, C., Soudine, A., and Ziveri, P.: The role of atmospheric deposition  
688 in the biogeochemistry of the Mediterranean Sea, *Prog. Oceanogr.*, 44, 147-190,  
689 doi:10.1016/S0079-6611(99)00024-5, 1999.

690 Guieu, C., Ridame, C., Pulido-Villena, E., Bressac, M., Desboeufs, K., and Dulac, F.: Impact of dust  
691 deposition on carbon budget: a tentative assessment from a mesocosm approach, *Biogeosci.*, 11,  
692 5621-5635, doi:10.5194/bg-11-5621-2014, 2014.

693 Hamonou, E., Chazette, P., Balis, D., Dulac, F., Schneider, X., Galani, E., Ancellet, G., and Papayannis,  
694 A.: Characterization of the vertical structure of Saharan dust export to the Mediterranean basin, *J.*  
695 *Geophys. Res.*, 104, 22257-22270, doi:10.1029/1999JD900257, 1999.

696 Hashimoto, M., Nakajima, T., Dubovik, O., Campanelli, M., Che, H., Khatri, P., Takamura, T., and  
697 Pandithurai, G.: Development of a new data-processing method for SKYNET sky radiometer  
698 observations, *Atmos. Meas. Tech.*, 5, 2723-2737, doi:10.5194/amt-5-2723-2012, 2012.

699 Haywood, J., Francis, P., Osborne, S., Glew, M., Loeb, N., Highwood, E., Tanré, D., Myhre, G.,  
700 Formenti, P., and Hirst, E.: Radiative properties and direct radiative effect of Saharan dust  
701 measured by the C-130 aircraft during SHADE: 1. Solar spectrum, *J. Geophys. Res.*, 108, 8577,  
702 doi:10.1029/2002JD002687, 2003.

703 Herut, B., Krom, M. D., Pan, G., and Mortimer, R.: Atmospheric input of nitrogen and phosphorus to  
704 the Southeast Mediterranean: Sources, fluxes and possible impact, *Limnol. Oceanogr.*, 44, 1683-  
705 1692, doi:10.4319/lo.1999.44.7.1683, 1999.

706 Jaenicke, R.: Aerosol physics and chemistry, in *Landolt-Börnstein Numerical Data and Functional*  
707 *Relationships in Science and Technology V, 4b*, edited by Fischer, G., 391-457, Springer-Verlag,  
708 Berlin, doi:10.1007/b31154, 1987.

709 Jeong, G. Y., Kim, J. Y., Seo, J., Kim, G. M., Jin, H. C., and Chun, Y.: Long-range transport of giant  
710 particles in Asian dust identified by physical, mineralogical, and meteorological analysis, *Atmos.*  
711 *Chem. Phys.*, 14, 505-521, doi:10.5194/acp-14-505-2014, 2014.

712 Johnston, A. M., Vincent, J. H., and Jones, A. D.: Electrical charge characteristics of dry aerosols  
713 produced by a number of laboratory mechanical dispersers, *Aerosol Sci. Technol.*, 6, 115-127,  
714 doi:10.1080/02786828708959125, 1987.

715 Li, X., Xingcai, L., and Xiaojing, Z. : Attenuation of an electromagnetic wave by charged dust particles  
716 in a sandstorm, *Appl. Opt.*, 49, 6756-6761, doi:10.1364/AO.49.006756, 2010.

717 Li, Z., Lau, W. K.-M., Ramanathan, V., Wu, G., Ding, Y., Manoj, M. G., Liu, J., Qian, Y., Li, J., Zhou, T.,  
718 Fan, J., Rosenfeld, D., Ming, Y., Wang, Y., Huang, J., Wang, B., Xu, X., Lee, S.-S., Cribb, M., Zhang, F.,  
719 Yang, X., Zhao, C., Takemura, T., Wand, K., Xia, X., Yin, Y., Zhang, H., Guo, J., Zhai, P. M., Sugimoto,  
720 N., Babu, S. S., and Brasseur, G. P.: Aerosol and monsoon climate interactions over Asia, *Rev.*  
721 *Geophys.*, 54, 866-929, doi:10.1002/2015RG000500, 2016.

722 Linke, C., Möhler, O., Veres, A., Mohácsi, A., Bozóki, Z., Szabó, G., and Schnaiter, M.: Optical  
723 properties and mineralogical composition of different Saharan mineral dust samples: a laboratory  
724 study, *Atmos. Chem. Phys.*, 6, 3315–3323, doi:10.5194/acp-6-3315-2006, 2006.

725 Liu, J., Zheng, Y., Li, Z., Flynn, C., Welton, E. J., and Cribb, M.: Transport, vertical structure and  
726 radiative properties of dust events in southeast China determined from ground and space  
727 sensors, *Atmos. Environ.*, 45, 6469–6480, doi:10.1016/j.atmosenv.2011.04.031, 2011.

728 Loÿe-Pilot, M. D., Martin, J. M., and Morelli, J.: Influence of Saharan dust on the rain acidity and  
729 atmospheric input to the Mediterranean, *Nature*, 321, 427–428, doi:10.1038/321427a0, 1986.

730 Lurton, T., Renard, J.-B., Vignelles, D., Jeannot, M., Akiki, R., Mineau, J.-L., and Tonnelier, T.: Light  
731 scattering at small angles by atmospheric irregular particles: modelling and laboratory  
732 measurements, *Atmos. Meas. Tech.*, 7, 931–939, doi:10.5194/amt-7-931-2014, 2014.

733 Maher, B. A., Prospero, J. M., Mackie, D., Gaiero, D., Hesse, P. P., and Balkanski, Y.: Global  
734 connections between aeolian dust, climate and ocean biogeochemistry at the present day and at  
735 the last glacial maximum, *Earth Sci. Rev.*, 99, 61–97, doi:10.1016/j.earscirev.2009.12.001, 2010.

736 Mahowald, N., Engelstaedter, S., Luo, C., Sealy, A., Artaxo, P., Benitez-Nelson, C., Bonnet, S., Chen,  
737 Y., Chuang P. Y., Cohen, D. D., Dulac, F., Herut, B., Johansen, A. M., Kubilay, N., Losno, R.,  
738 Maenhaut, W., Paytan, A., Prospero, J. M., Shank, L. M., and Siefert, R. L.: Atmospheric Iron  
739 deposition: global distribution, variability and human perturbations, *Annu. Rev. Mar. Sci.*, 1, 245–  
740 278, doi:10.1146/annurev-marine.010908.163727, 2009.

741 Mahowald, N., Ward, D. S., Kloster, S., Flanner, M. G., Heald, C. L., Heavens, N. G., Hess, P. G.,  
742 Lamarque, J.-F., and Chuang P. Y.: Aerosol impacts on climate and biogeochemistry, *Annu. Rev.*  
743 *Environ. Resour.*, 36, 45–74, doi:10.1146/annurev-environ-042009-0945072011, 2011.

744 Mallet, M., Dulac, F., Formenti, P., Nabat, P., Sciare, J., Roberts, G., Pelon, J., Ancellet, G., Tanré, D.,  
745 Parol, F., Denjean, C., Brogniez, G., di Sarra, A., Alados-Arboledas, L., Arndt, J., Auriol, F., Blarel, L.,  
746 Bourriane, T., Chazette, P., Chevaillier, S., Claeys, M., D'Anna, B., Derimian, Y., Desboeufs, K., Di  
747 Iorio, T., Doussin, J.-F., Durand, P., Féron, A., Freney, E., Gaimoz, C., Goloub, P., Gómez-Amo, J. L.,  
748 Granados-Muñoz, M. J., Grand, N., Hamonou, E., Jankowiak, I., Jeannot, M., Léon, J.-F., Maillé, M.,  
749 Mailler, S., Meloni, D., Menut, L., Momboisse, G., Nicolas, J., Podvin, T., Pont, V., Rea, G., Renard,  
750 J.-B., Roblou, L., Schepanski, K., Schwarzenboeck, A., Sellegri, K., Sicard, M., Solmon, F., Somot, S.,  
751 Torres, B., Totems, J., Triquet, S., Verdier, N., Verwaerde, C., Waquet, F., Wenger, J., and Zapf, P.:  
752 Overview of the Chemistry-Aerosol Mediterranean Experiment/Aerosol Direct Radiative Forcing  
753 on the Mediterranean Climate (ChArMEx/ADRIMED) summer 2013 campaign, *Atmos. Chem.*  
754 *Phys.*, 16, 455–504, doi:10.5194/acp-16-455-2016, 2016.

755 Maring, H., Savoie, D. L., Izaguirre, M. A., Custals, L., and Reid, J. S.: Mineral dust aerosol size  
756 distribution change during atmospheric transport, *J. Geophys. Res.*, 108, 8592,  
757 doi:10.1029/2002JD002536, 2003.

758 Martin, J., Gordon, R. M., and Fitzwater, S. E.: The case for iron, *Limnol. Oceanogr.*, 36, 1793–1802,  
759 doi:10.4319/lo.1991.36.8.1793, 1991.

760 McConnell, C. L., Highwood, E. J., Coe, H., Formenti, P., Anderson, B., Osborne, S., Nava, S.,  
761 Desboeufs, K., Chen, G., and Harrison, M. A. J.: Seasonal variations of the physical and optical  
762 characteristics of Saharan dust: Results from the Dust Outflow and Deposition to the Ocean  
763 (DODO) experiment, *J. Geophys. Res.*, 113, D14S05, doi:10.1029/2007JD009606, 2008.

764 Middleton, N. J., Betzer, P. R., and Bull, P. A.: Long-range transport of ‘giant’ aeolian quartz grains:  
765 linkage with discrete sedimentary sources and implications for protective particle transfer, *Mar.*  
766 *Geol.*, 177, 411–417, doi:10.1016/S0025-3227(01)00171-2, 2001.

767 Morales-Baquero, R., Pulido-Villena, E., and Reche, I.: Atmospheric inputs of phosphorus and  
768 nitrogen to the southwest Mediterranean region: Biogeochemical responses of high mountain  
769 lakes, *Limnol. Oceanogr.*, 51, 830–837, doi:10.4319/lo.2006.51.2.0830, 2006.

770 Moulin, C., Lambert, C. E., Dayan, U., Masson, V., Ramonet, M., Bousquet, P., Legrand, M., Balkanski,  
771 Y. J., Guelle, W., Marticorena, B., Bergametti, G., and Dulac, F.: Satellite climatology of African  
772 dust transport in the Mediterranean atmosphere, *J. Geophys. Res.*, 103, 13137–13144,  
773 doi:10.1029/98JD00171, 1998.

774 Nabat, P., Solmon, F., Mallet, M., Kok, J. F. and Somot, S. : Dust emission size distribution impact on  
775 aerosol budget and radiative forcing over the Mediterranean region: a regional climate model  
776 approach, *Atmos. Chem. Phys.*, 12, 10545-10567, 10.5194/acp-12-10545-2012, 2012.

777 Nabat, P.; Somot, S.; Mallet, M.; Chiapello, I.; Morcrette, J. J., Solmon, F., Szopa, S., Dulac, F., Collins,  
778 W., Ghan, S., Horowitz, L. W., Lamarque, J. F., Lee, Y. H., Naik, V., Nagashima, T., Shindell, D., and  
779 Skeie, R.: A 4-D climatology (1979-2009) of the monthly tropospheric aerosol optical depth  
780 distribution over the Mediterranean region from a comparative evaluation and blending of  
781 remote sensing and model products, *Atmos. Meas. Tech.*, 6, 1287-1314, doi:10.5194/amt-6-1287-  
782 2013, 2013.

783 Nabat, P., Somot, S., Mallet, M., Michou, M., Sevault, F., Driouech, F., Meloni, D., di Sarra, A., Di  
784 Biagio, C., Formenti, P., Sicard, M., Léon, J.-F., and Bouin, M.-N.: Dust aerosol radiative effects  
785 during summer 2012 simulated with a coupled regional aerosol-atmosphere-ocean model over  
786 the Mediterranean, *Atmos. Chem. Phys.*, 15, 3303-3326, doi:10.5194/acp-15-3303-2015, 2015a.

787 Nabat, P., Somot, S., Mallet, M., Sevault, F., Chiacchio, M., and Wild, M.: Direct and semi-direct  
788 aerosol radiative effect on the Mediterranean climate variability using a coupled regional climate  
789 system model, *Clim. Dyn.*, 44, 1127-1155, doi:10.1007/s00382-014-2205-6, 2015b.

790 Nicoll, K. A., Harrison, R. G., and Ulanowski, Z.: Observations of Saharan dust layer electrification,  
791 *Environ. Res. Lett.*, 6, 014001, doi:10.1088/1748-9326/6/1/014001, 2011.

792 Nihlén, T., Mattsson, J. O., Rapp, A., Gagaoudaki, C., Kornaros, G., and Papageorgiou, J.: Monitoring  
793 of Saharan dust fallout on Crete and its contribution to soil formation. *Tellus B*, 47: 365–374.  
794 doi:10.1034/j.1600-0889.47.issue3.7.x, 1995.

795 Omar, A. H., Winker, D. M., Kittaka, C., Vaughan, M. A., Liu, Z., Hu, Y., Trepte, C. R., Rogers, R. R.,  
796 Ferrare, R. A., Lee, K.-P., Khuen, R. E., and Hostetler, C. A.: The CALIPSO automated aerosol  
797 classification and lidar ratio selection algorithm, *J. Atmos. Oceanic Technol.*, 26, 1994-2014,  
798 doi:10.1175/2009JTECHA1231.1, 2009.

799 Pey, J., Querol, X., Alastuey, A., Forastiere, F., and Stafoggia, M.: African dust outbreaks over the  
800 Mediterranean Basin during 2001–2011: PM<sub>10</sub> concentrations, phenomenology and trends, and its  
801 relation with synoptic and mesoscale meteorology, *Atmos. Chem. Phys.*, 13, 1395-1410,  
802 doi:10.5194/acp-13-1395-2013, 2013.

803 Prodi, F. and Fea, G.: A case of transport and deposition of Saharan dust over the Italian Peninsula  
804 and southern Europe, *J. Geophys. Res.*, 84, 6951–6960, doi:10.1029/JC084iC11p06951, 1979.

805 Prospero, J. M., Bonatti, E., Schubert, C., and Carlson, T. N.: Dust in the Caribbean atmosphere traced  
806 to an African dust storm, *Earth Planet. Sci. Lett.*, 9, 287-293, doi:10.1016/0012-821X(70)90039-7,  
807 1970.

808 Prospero, J. M. and Carlson, T. N.: Saharan dust outbreaks over the tropical North Atlantic, *Pure Appl.*  
809 *Geophys.*, 119, 677-691, doi:10.1007/BF00878167, 1981.

810 Pye, K.: Aeolian dust transport and deposition over Crete and adjacent parts of the Mediterranean  
811 Sea, *Earth Surf. Proc. Land.*, 17, 271–288. doi:10.1002/esp.3290170306, 1992.

812 Querol, X., Pey, J., Pandolfi, M., Alastuey, A., Cusack, M., Pérez, N., Moreno, T., Viana, M.,  
813 Mihalopoulos, N., Kallos, G., and Kleanthous, S.: African dust contributions to mean ambient PM<sub>10</sub>  
814 mass-levels across the Mediterranean Basin, *Atmos. Environ.*, 43, 4266-4277,  
815 doi:10.1016/j.atmosenv.2009.06.013, 2009.

816 Rea, G., Turquety, S., Menut, L., Briant, R., Mailler, S., and Siour, G.: Source contributions to 2012  
817 summertime aerosols in the Euro-Mediterranean region, *Atmos. Chem. Phys.*, 15, 8013-8036,  
818 doi:10.5194/acp-15-8013-2015, 2015.

819 Reche, I., Ortega-Retuerta, E., Romera O., Pulido Villena, E., Morales Baquero, R., and Casamayor, E.  
820 O.: Effect of Saharan dust inputs on bacterial activity and community composition in  
821 Mediterranean lakes and reservoirs, *Limnol. Oceanogr.*, 54, 869-879,  
822 doi:10.4319/lo.2009.54.3.0869, 2009.

823 Reid, J. S., Kinney, J. E., Westphal, D. L., Holben, B. N., Welton, E. J., Tsay, S.-C., Eleuterio, D. P.,  
824 Campbell, J. R., Christopher, S. A., Colarco, P. R., Jonsson, H. H., Livingston, J. M., Maring, H. B.,  
825 Meier, M. L., Pilewski, P., Prospero, J. M., Reid, E. A., Remer, L. A., Russel, P. B., Savoie, D. L.,



826 Smirnov, A., and Tanré, D.: Analysis of measurements of Saharan dust by airborne and ground-  
827 based remote sensing methods during the Puerto Rico Dust Experiment (PRIDE), *J. Geophys. Res.*,  
828 108, 8586, doi:10.1029/2002JD002493, 2003a.

829 Reid, J. S., Jonsson, H. H., Maring, H. B., Smirnov, A., Savoie, D. L., Cliff, S. S., Reid, E. A., Livingston, J.  
830 M., Meier, M. M., Dubovik, O., and Tsay, S.-C.: Comparison of size and morphological  
831 measurements of coarse mode dust particles from Africa, *J. Geophys. Res.*, 108, 8593,  
832 10.1029/2002JD002485, 2003b.

833 Reiff, J., Forbes, G. S., Spijksma, F. Th. M., and Reynders, J. J.: African dust reaching northwestern  
834 Europe: A case study to verify trajectory Calculations, *J. Clim. Appl. Meteor.*, 25, 1543-1567,  
835 doi:10.1175/1520-0450(1986)025<1543:ADRNEA>2.0.CO;2, 1986.

836 Renard, J.-B. Francis, M., Hadamcik, E., Dugeron, D., Couté, B., Gaubicher, B., and Jeannot, M.:  
837 Scattering properties of sand. 2. Results for sands from different origins, *Appl. Opt.*, 49, 3552-  
838 3559, doi:10.1364/AO.49.003552, 2010.

839 Renard, J.-B., Dulac, F., Berthet, G., Lurton, T., Vignelles, D., Jégou, F., Tonnelier, T., Jeannot, M.,  
840 Couté, B., Akiki, R., Verdier, N., Mallet, M., Gensdarmes, F., Charpentier, P., Mesmin, S., Duverger,  
841 V., Dupont, J.-C., Elias, T., Crenn, V., Sciare, J., Zieger, P., Salter, M., Roberts, T., Giacomoni, J.,  
842 Gobbi, M., Hamonou, E., Olafsson, H., Dagsson-Waldhauserova, P., Camy-Peyret, C., Mazel, C.,  
843 Décamps, T., Piringer, M., Surcin, J., and Dugeron, D.: LOAC, a light aerosols counter for ground-  
844 based and balloon measurements of the size distribution and of the main nature of atmospheric  
845 particles, 1. Principle of measurements and instrument evaluation, *Atmos. Meas. Tech.*, 9, 1721-  
846 1742, doi:10.5194/amt-9-1721-2016, 2016a.

847 Renard, J.-B., Dulac, F., Berthet, G., Lurton, T., Vignelles, D., Jégou, F., Tonnelier, T., Jeannot, M.,  
848 Couté, B., Akiki, R., Verdier, N., Mallet, M., Gensdarmes, F., Charpentier, P., Mesmin, S., Duverger,  
849 V., Dupont, J.-C., Elias, T., Crenn, V., Sciare, J., Zieger, P., Salter, M., Roberts, T., Giacomoni, J.,  
850 Gobbi, M., Hamonou, E., Olafsson, H., Dagsson-Waldhauserova, P., Camy-Peyret, C., Mazel, C.,  
851 Décamps, T., Piringer, M., Surcin, J., and Dugeron, D.: LOAC, a light aerosols counter for ground-  
852 based and balloon measurements of the size distribution and of the main nature of atmospheric  
853 particles, 2. First results from balloon and unmanned aerial vehicle flights, *Atmos. Meas. Tech.*, 9,  
854 3673-3686, doi:10.5194/amt-9-3673-2016, 2016b.

855 Ryder, C. L., Highwood, E. J., Lai, T. M., Sodemann, H. and Marsham, J. H.: Impact of atmospheric  
856 transport on the evolution of microphysical and optical properties of Saharan dust, *Geophys. Res.*  
857 *Lett.*, 40, 2433–2438, doi:10.1002/grl.50482, 2013.

858 Schmid, B., Livingston, J. M., Russell, P. B., Durkee, P. A., Jonsson, H. H., Collins, D. R., Flagan, R. C.,  
859 Seinfeld, J. H., Gassó, S., Hegg, D. A., Öström, E., Noone, K. J., Welton, E. J., Voss, K. J., Gordon, H.  
860 R., Formenti, P., and Andreae, M. O.: Clear-sky closure studies of lower tropospheric aerosol and  
861 water vapor during ACE-2 using airborne sunphotometer, airborne in-situ, space-borne, and  
862 ground-based measurements., *Tellus B*, 52, 568–593. doi:10.1034/j.1600-0889.2000.00009.x,  
863 2000.

864 Schütz, L., Jaenicke, R., and Pietrek, H.: Saharan dust transport over the North Atlantic Ocean, *Geol.*  
865 *Soc. Am. Spec. Pap.*, 186, 87-100, doi:10.1130/SPE186-p87, 1981.

866 Slinn, W. G. N.: Air to sea transfer of particles, in *Air-sea exchange of gases and particles*, Liss, P. S.,  
867 and Slinn, W. G. N. Eds., N.A.T.O. AS1 Series, Reidel, Dordrecht, Holland, 299-396, 1983.

868 Sow, M., Crase, E., Rajot, J. L., Sankaran, R. M., and Lacks, D. J.: Electrification of particles in dust  
869 storms: Field measurements during the monsoon period in Niger, *Atmos. Res.*, 102, 343-350,  
870 doi:10.1016/j.atmosres.2011.08.010, 2011.

871 Stohl, A., Eckhardt, S., Forster, C., James, P., Spichtinger, N., and Seibert, P.: A replacement for simple  
872 back trajectory calculations in the interpretation of atmospheric trace substance measurements,  
873 *Atmos. Environ.*, 36, 4635–4648, doi:10.1016/S1352-2310(02)00416-8, 2002.

874 Stokes, G. G.: On the effect of the internal friction of fluids on the motion of pendulums, *Trans.*  
875 *Cambridge Philos. Soc.*, 9, 51-52, 1851.

876 Swap, R., Garstang, M., Greco, S., Talbot, R. and Kållberg, P.: Saharan dust in the Amazon Basin, *Tellus*  
877 *B*, 44, 133–149, doi:10.1034/j.1600-0889.1992.t01-1-00005.x, 1992.

878 Thieuleux, F., Moulin, C., Bréon, F.M., Maignan, F., Poitou, J., and Tanré, D.: Remote sensing of  
879 aerosols over the oceans using MSG/SEVIRI imagery, *Ann. Geophys.*, 23, 3561-3568,  
880 doi:10.5194/angeo-23-3561-2005, 2005.

881 Ulanowski, Z., Bailey, J., Lucas, P.W., Hough, J.H., and Hirst, E.: Alignment of atmospheric mineral  
882 dust due to electric field, *Atmos. Chem. Phys.*, 7, 6161-6173, doi:10.5194/acp-7-6161-2007, 2007.

883 Vincent, J., Laurent, B., Losno, R., Bon Nguyen, E., Roullet, P., Sauvage, S., Chevaillier, S., Coddeville,  
884 P., Ouboulmane, N., di Sarra, A. G., Tovar-Sánchez, A., Sferlazzo, D., Massanet, A., Triquet, S.,  
885 Morales Baquero, R., Fournier, M., Coursier, C., Desboeufs, K., Dulac, F., and Bergametti, G.:  
886 Variability of mineral dust deposition in the western Mediterranean basin and south-east of  
887 France, *Atmos. Chem. Phys.*, 16, 8749-8766, doi:10.5194/acp-16-8749-2016, 2016.

888 Weinzierl, B., Petzold, A., Esselborn, M., Wirth, M., Rasp, K., Kandler, K., Schütz, L., Koepke, P., and  
889 Fiebig, M.: Airborne measurements of dust layer properties, particle size distribution and mixing  
890 state of Saharan dust during SAMUM 2006, *Tellus B*, 61, 96–117, 2009.

891 Weinzierl, B., Sauer, D., Esselborn, M., Petzold, A., Veira, A., Rose, M., Mund, S., Wirth, M., Ansmann,  
892 A., Tesche, M., Gross, S., and Freudenthaler, V.: Microphysical and optical properties of dust and  
893 tropical biomass burning aerosol layers in the Cape Verde region—an overview of the airborne in  
894 situ and lidar measurements during SAMUM-2, *Tellus B*, 63, 589-618, doi:10.1111/j.1600-  
895 0889.2011.00566.x, 2011.

896 Weiss-Wrana, K.: Optical properties of interplanetary dust - Comparison with light scattering by  
897 larger meteoritic and terrestrial grains, *Astron. Astrophys.*, 126, 240-250, 1983.

898 Winker, D. M., Vaughan, M. A., Omar, A., Hu, Y., Powell, K. A., Liu, Z., Hunt, W. H., and Young, S. A.:  
899 Overview of the CALIPSO mission and CALIOP data processing algorithms, *J. Atmos. Oceanic*  
900 *Technol.*, 26, 2310-2323, doi:10.1175/2009JTECHA1281.1, 2009.

901 Zannoni, N., Gros, V., Sarda Esteve, R., Kalogridis, C., Michoud, V., Dusanter, S., Sauvage, S., Locoge,  
902 N., Colomb, A., and Bonsang, B.: Summertime OH reactivity from a receptor coastal site in the  
903 Mediterranean basin, *Atmos. Chem. Phys. Discuss.*, doi:10.5194/acp-2016-684, submitted, 2017.

904 Zender, C. S., H. Bian, and D. Newman, Mineral Dust Entrainment and Deposition (DEAD) model:  
905 Description and 1990s dust climatology, *J. Geophys. Res.*, 108(D14), 4416,  
906 doi:10.1029/2002JD002775, 2003.

907  
 908  
 909  
 910  
 911  
 912  
 913  
 914  
 915  
 916  
 917  
 918  
 919  
 920  
 921  
 922  
 923  
 924  
 925  
 926  
 927  
 928  
 929  
 930  
 931  
 932  
 933  
 934  
 935  
 936  
 937  
 938  
 939

Date (2013)	Time (UTC)		Altitude range (km)	Launch site
	start	end		
15 June	22:12	22:48	0.9 – 6.9	
16 June	10:37	11:14	2.0 – 12.1	
16 June	21:17	21:59	0.2 – 10.1	
17 June	10:02	10:41	0.1 – 11.4	
17 June	18:29	20:33	0.9 – 33.3	Cap d'en Font, Minorca Isl., Spain (39.88°N, 4.25°E)
18 June	16:35	18:41	0.2 – 35.4	
18 June	21:19	22:39	0.4 – 21.5	
19 June	10:15	12:03	0.8 – 30.7	
19 June	13:50	15:03	0.3 – 20.7	
28 June	05:38	07:54	0.6 – 36.0	
29-30 June	23:31	01:49	0.2 – 35.9	
30 June	14:03	15:46	0.1 – 26.8	
2 July	10:30	12:24	0.7 – 32.8	
27-28 July	23:13	01:17	0.3 – 33.5	Levant Isl., France (43.02°N, 6.46°E)
28 July	15:31	18:06	0.3 – 33.3	
3 August	11:04	12:35	0.3 – 21.7	
4 August	15:32	17:36	0.2 – 32.2	

**Table 1.** List of the 17 LOAC flights under Light Dilatable Balloons (LDB) flown during African dust plume events of the ChArMEx summer 2013 campaign.

Balloon #	Date (2013)	Time slot of LOAC data (UTC)		Drift altitude (km)	Latitude, longitude at end of flight	Flight length (km)	Ceiling duration (h)
		start	end				
B74	16 June	10:00	21:28	2.1	42.892°N, 05.229°E	361	11.3
B70	16 June	09:51	23:01	3.1	40.182°N, 06.128°E	164	12.6
B75	17 June	09:31	16:23	2.0	42.815°N, 03.811°E	362	6.4
B72	17 June	17:11	18:59	2.75	43.179°N, 04.800°E	377	7.0
B77	19 June	10:25	16:54	2.55	43.042°N, 04.833°E	369	6.0
B71	19 June	10:29	15:58	3.3	43.041°N, 05.151°E	363	3.6
B80	27-28 June	09:50	12:31	3.0	37.916°N, 12.145°E	719	25.3
B73	28 June	05:25	16:42	2.7	37.523°N, 08.830°E	512	11.2
B76	2-3 July	13:04	09:14	3.2	37.880°N, 12.109°E	717	19.3
B82	3 August	06:12	08:12	3.0	43.077°N, 06.662°E	45	1.4

941

942 **Table 2.** List of the 10 LOAC flights aboard drifting Boundary Layer Pressurized Balloons (BLPBs) flown  
943 during African dust plume events of the ChArMEx summer 2013 campaign. All balloons were  
944 launched from Minorca Isl. (Spain; 39.864°N, 4.255°N) except B82 that was launched from the Levant  
945 Isl. (France; 43.022°N, 6.460°E).

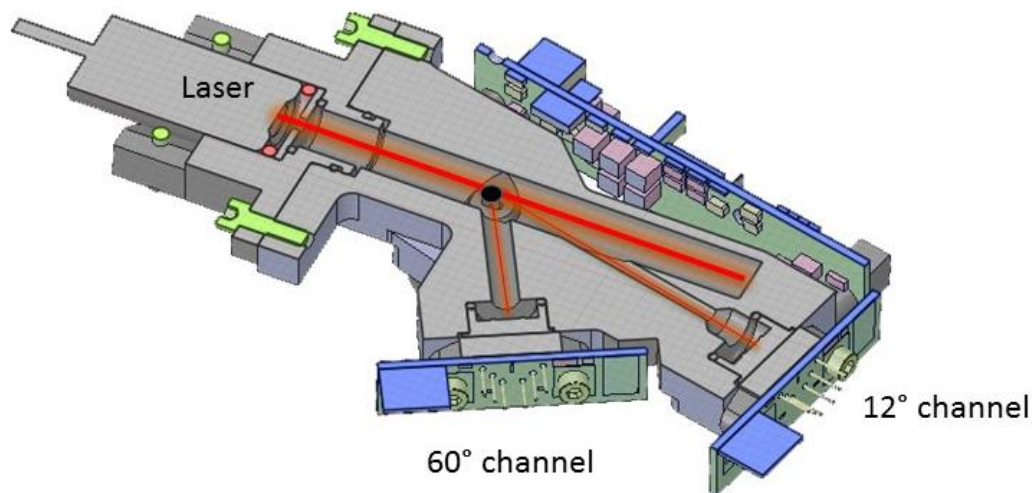
Date (2013)	Altitude (km)	Average volume median diameter ( $D_m$ , $\mu\text{m}$ ) $\pm$ standard deviation (number of measurements)		
		Mode 1	Mode 2	Mode 3
16 June	2.1	0.22 $\pm$ 0.02 (32)	3.6 $\pm$ 0.8 (32)	30.6 $\pm$ 3.4 (32)
	3.1	0.30 $\pm$ 0.07 (31)	3.3 $\pm$ 0.3 (31)	28.5 $\pm$ 1.7 (30)
17 June	2.0	0.26 $\pm$ 0.02 (17)	4.1 $\pm$ 0.6 (17)	27.4 $\pm$ 4.1 (17)
	2.8	0.24 $\pm$ 0.02 (16)	3.3 $\pm$ 0.5 (16)	30.9 $\pm$ 5.9 (16)
19 June	2.6	0.25 $\pm$ 0.01 (28)	3.5 $\pm$ 0.6 (28)	32.8 $\pm$ 4.7 (27)
	3.3	0.26 $\pm$ 0.01 (48)	4.5 $\pm$ 0.5 (48)	32.4 $\pm$ 4.2 (41)
Average		0.26 $\pm$ 0.04	3.7 $\pm$ 0.4	30.4 $\pm$ 2.8

947

948 **Table 3.** Average volume median diameter ( $D_m$ ) of the three fitted aerosol particle modes and  
 949 respective standard deviation along BPCL flights at float altitude within dust layers, for the 6 BPCLs  
 950 launched from Minorca during the 16-19 June 2013 dust event. The time evolution for the three pairs  
 951 of BPCL flights during this period is shown in Figure 16. The average and standard deviation in the  
 952 bottom line are obtained by averaging the 6 above values.

953

954



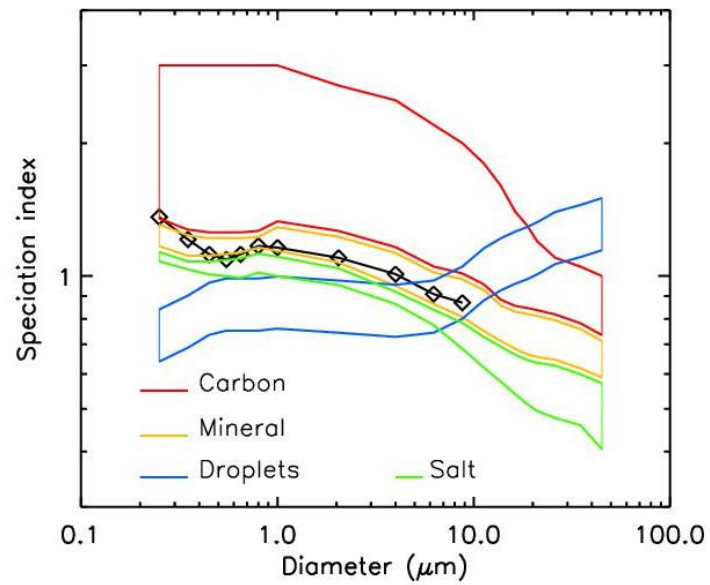
955

956

957

958

**Figure 1.** The LOAC instrument and principle of scattering measurements at two angles.



960

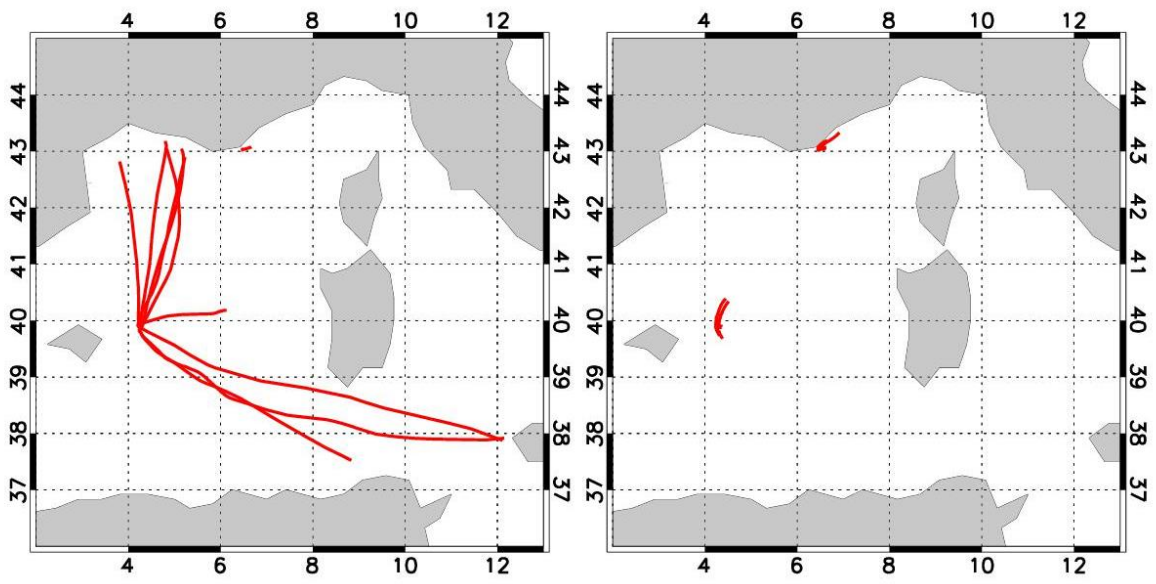
961

962 **Figure 2.** “Speciation zones” obtained in laboratory for several types of particles (color lines) and an  
963 example of LOAC speciation index obtained during ambient air measurements inside a Saharan dust  
964 plume at an altitude of 3.1 km (18 June 2013, 18:15 UT) above Minorca, Spain (diamonds).

965

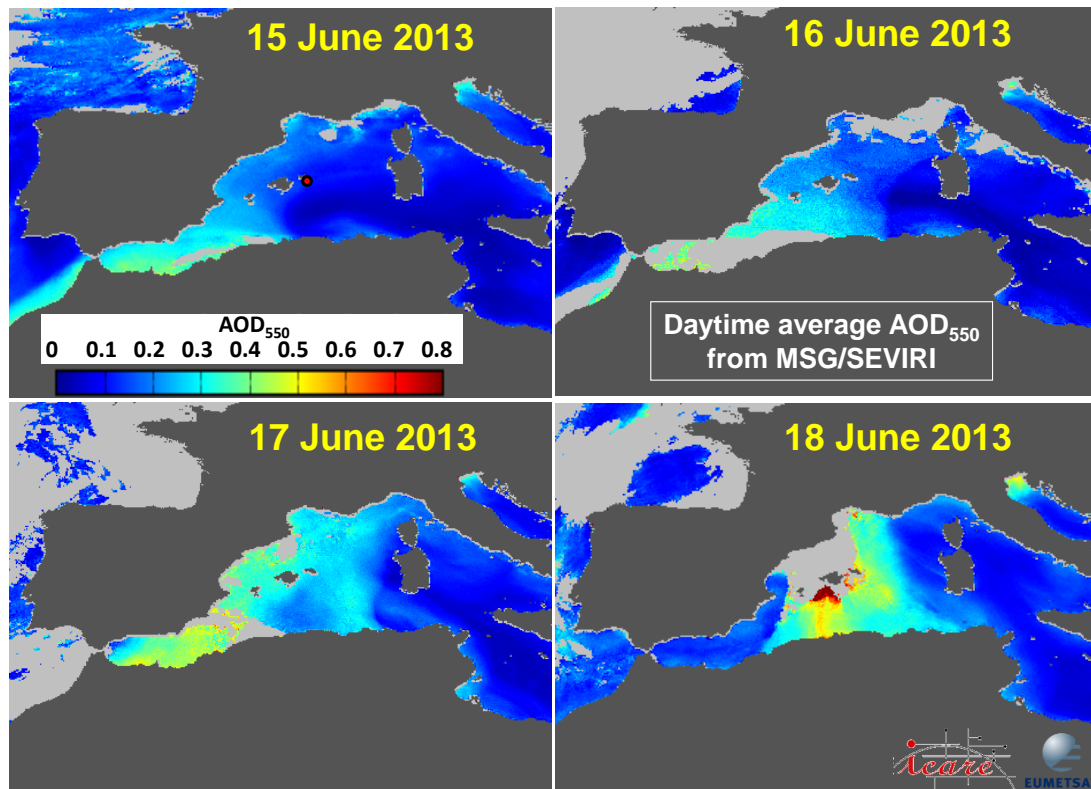
966

967



968  
969  
970  
971  
972

**Figure 3.** Trajectories of the flights for the 10 BLPBs (left) and 17 LDBs (right).



974

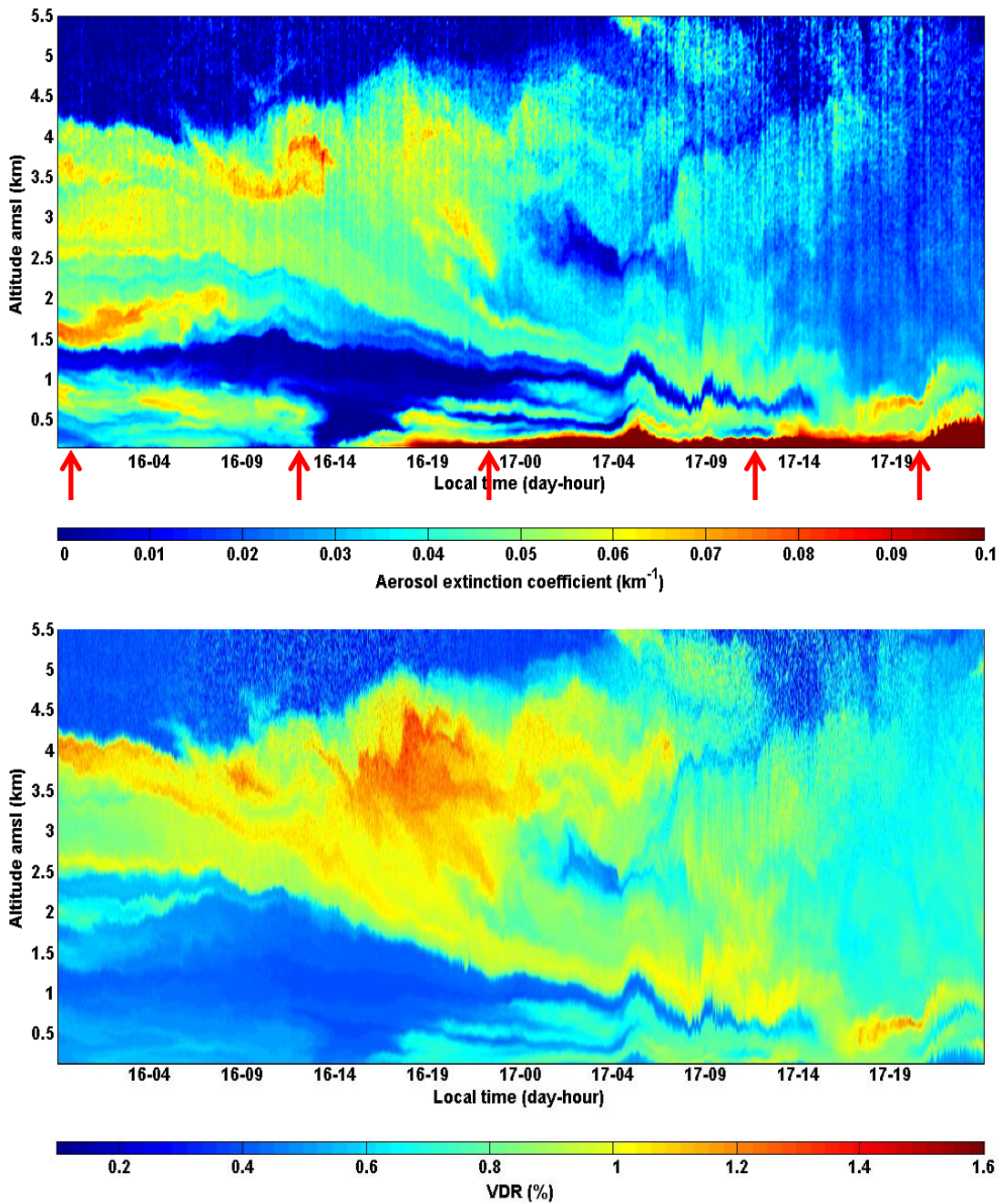
975

976 **Figure 4.** Daytime averaged MSG/SEVIRI-derived AOD at 550 nm over seawater from June 15 to 18,  
 977 2013, showing the synoptic development of the dust event. The product is computed by the ICARE  
 978 data and services center (<http://www.icare.univ-lille1.fr>) based on the algorithm of Thieuleux et al.  
 979 (2005). Lands are masked in dark grey and clouds over ocean in light grey. The red dot on the 15 June  
 980 image indicates the balloon launching site and remote sensing station on Minorca Island.

981

982





984

985

986 **Figure 5.** Lidar-derived time-height cross-sections of the aerosol extinction (top) and volume

987 depolarization ratio (bottom) at Minorca from June 15, 22:00 to 17, 24:00 UT. The red arrows

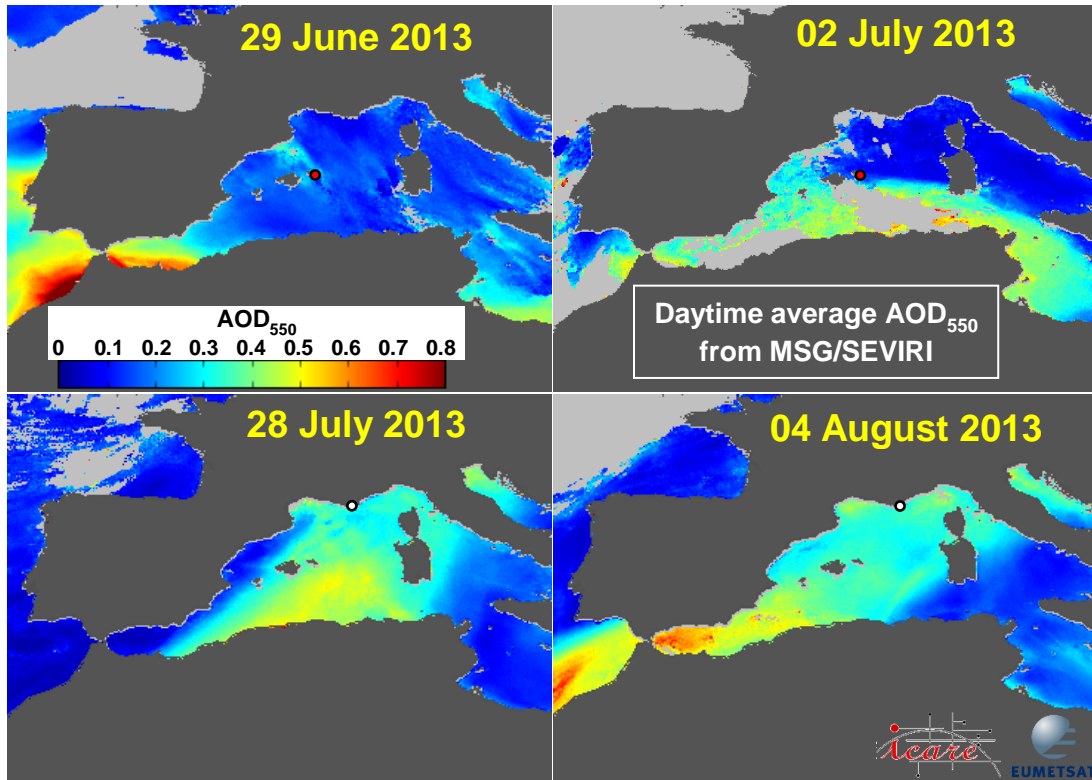
988 indicate the time of the 5 LDB launches. High depolarization ratio indicates desert dust. Courtesy of

989 P. Chazette and J. Totems, after Chazette et al. (2016).

990

991

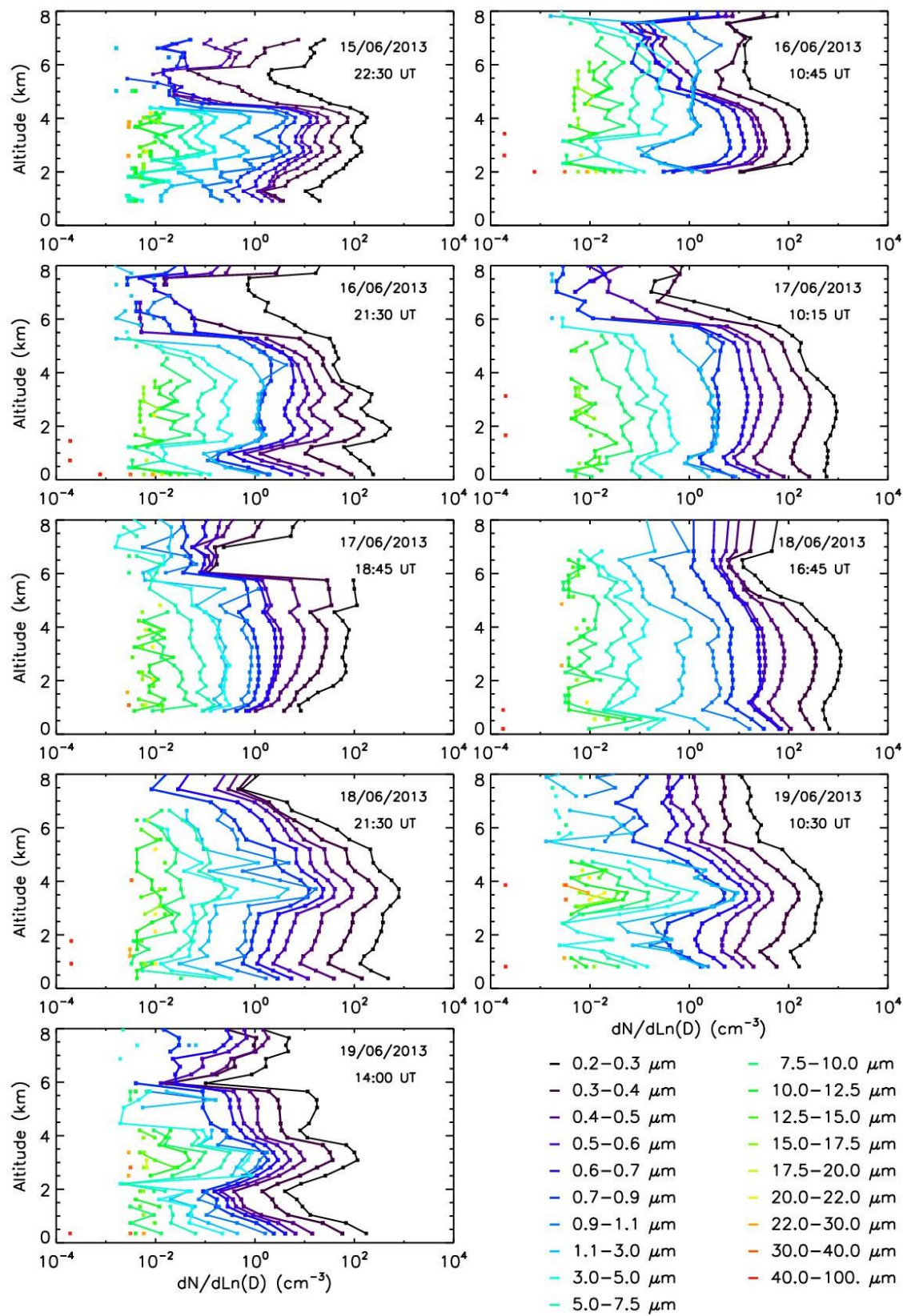
992



993  
994

995 **Figure 6.** Daytime averaged MSG/SEVIRI-derived AOD at 550 nm over seawater on 29 June, 2 and 28  
996 July, and 2 August 2013. The product is computed by the ICARE data and services center  
997 (<http://www.icare.univ-lille1.fr>) based on the algorithm of Thieuleux et al. (2005). Lands are masked  
998 in dark grey and clouds over ocean in light grey. The red dot on the 29 June and 2 July (top) images  
999 indicates the balloon launching site and remote sensing station on Minorca Island, and the white dot  
1000 on the 28 July and 2 August (bottom) images indicates the balloon launching site on the Levant  
1001 Island.

1002  
1003  
1004



1006

1007

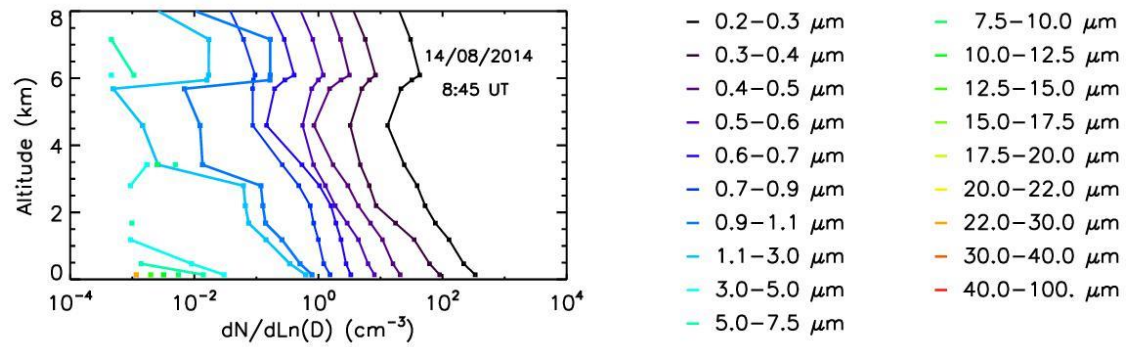
1008

1009

1010

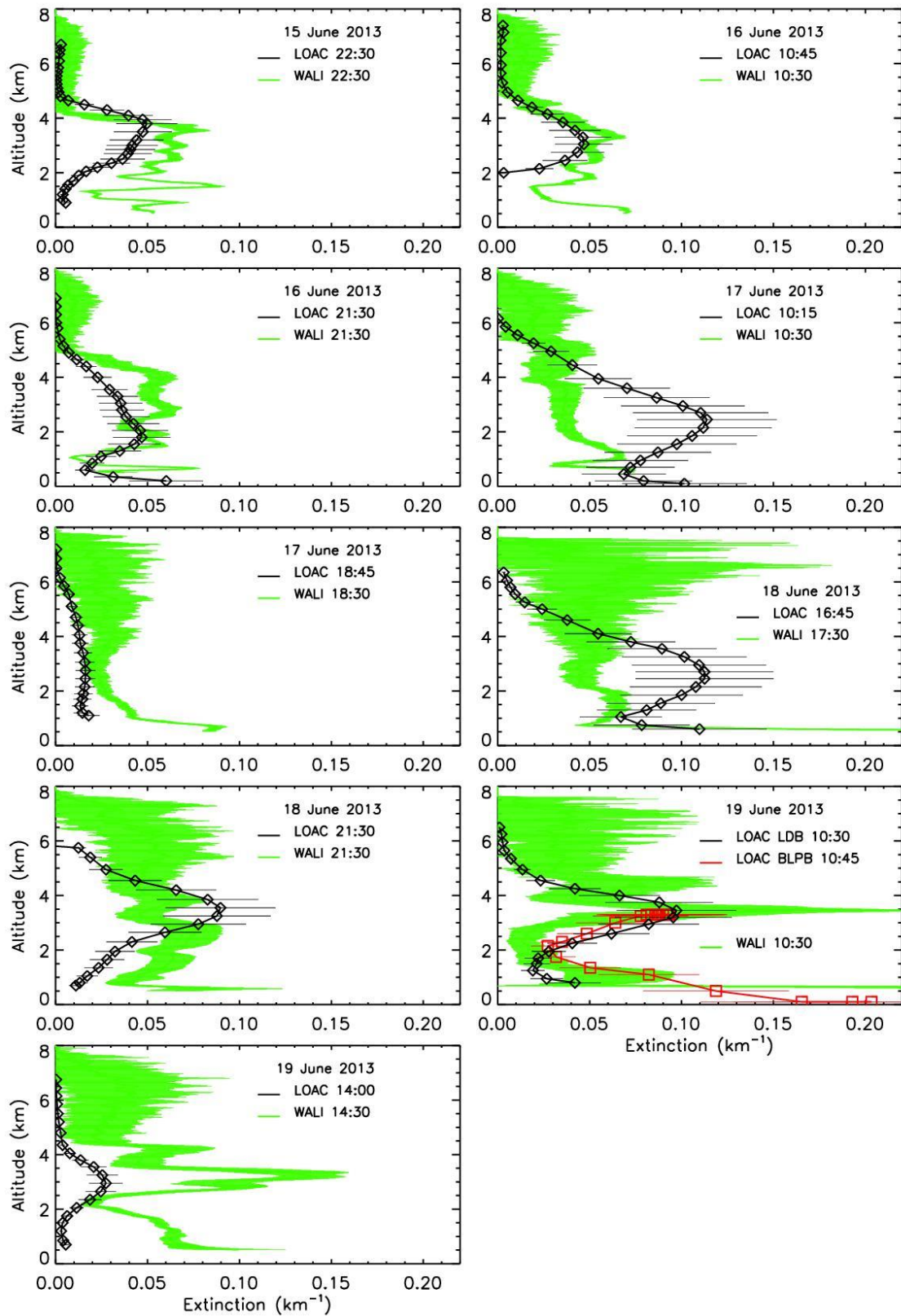
**Figure 7.** Evolution of the dust plume from LOAC balloon measurements over Minorca, Spain, from 15 to 19 June. The ascent from 0 to 8 km takes about 30 min and the reported times of measurement are taken at the middle of the profile.

1011



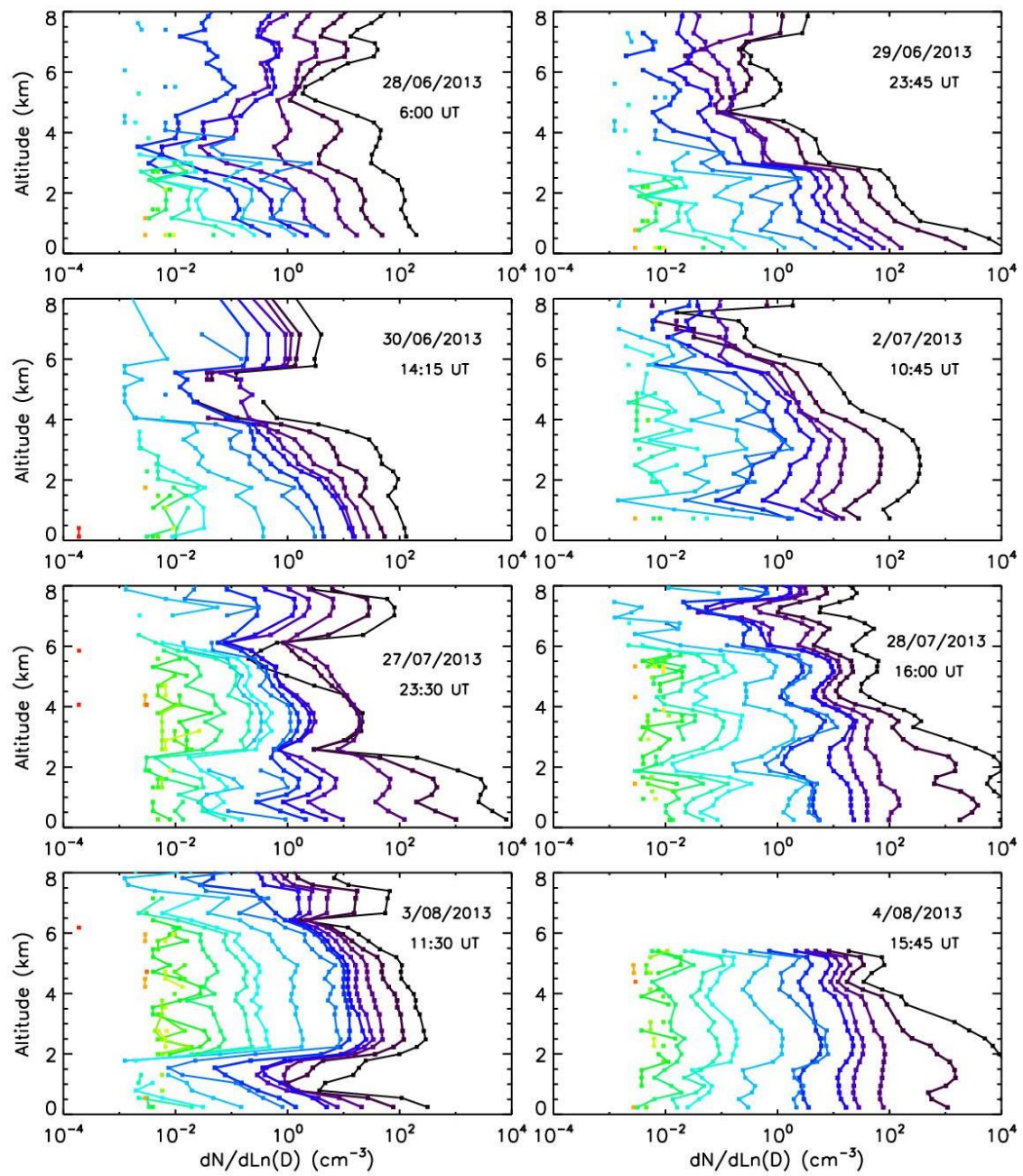
1012  
1013  
1014  
1015

**Figure 8.** Typical vertical profile when no dust is present; flight from Aire sur l'Adour (South West of France), on 14 August 2014.



1016  
 1017  
 1018  
 1019  
 1020

**Figure 9.** Comparison between LOAC extinctions and WALI lidar extinction at 350 nm. All the WALI profiles obtained between -30 min. and +30 min. of the given times are plotted. The LOAC error bars consider the uncertainty on the LOAC measurements and on the counting-extinction conversion; the WALI error bars are calculated from the individual measurement scatter.

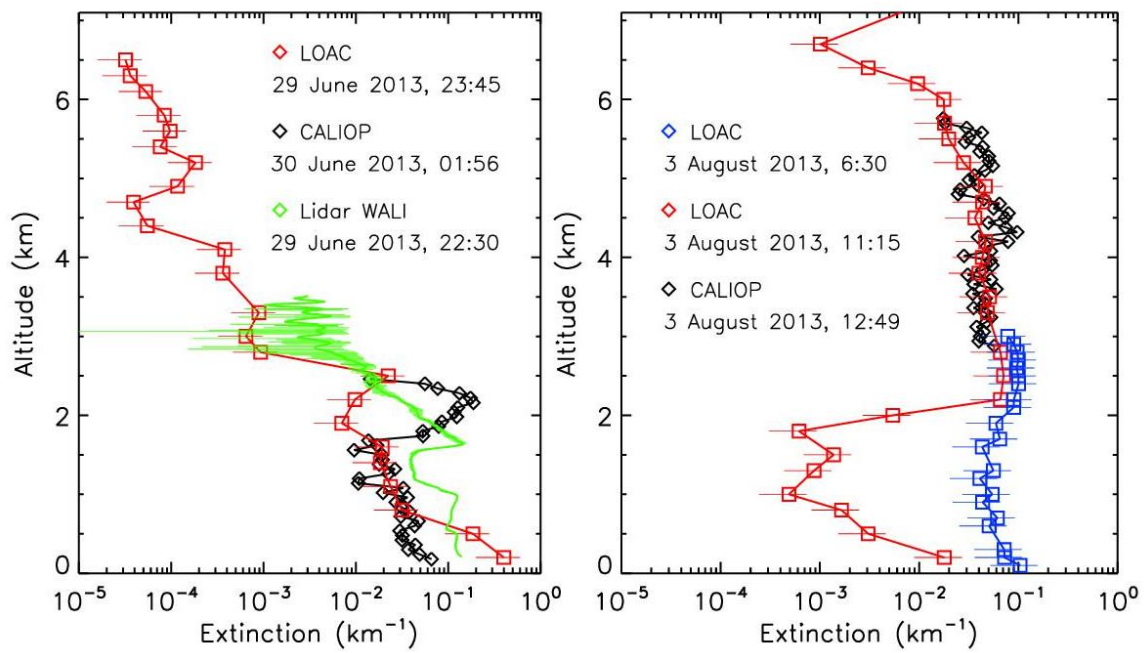


1022

1023

1024 **Figure 10.** Same as Fig. 7 but for other sand plume events observed over Minorca (27 June – 2 July)

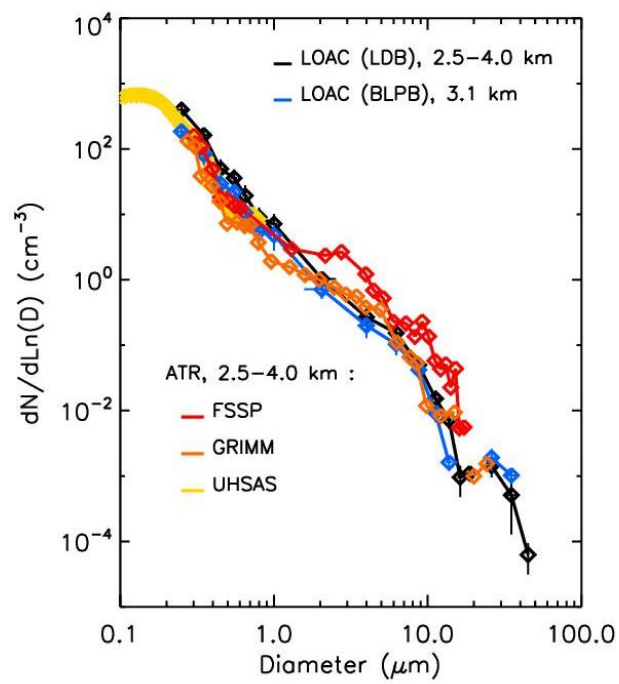
1025 and Ile du Levant (27 July - 4 August).



1027  
 1028  
 1029  
 1030  
 1031  
 1032  
 1033

**Figure 11.** Left, vertical profiles of aerosol extinction from LOAC, CALIOP and WALI for the 29-30 June event, above Minorca; right, vertical profiles of aerosol extinction from LOAC (LDB and BLPB flights) and CALIOP for the 3 August event above Ile du Levant.

1034



1035

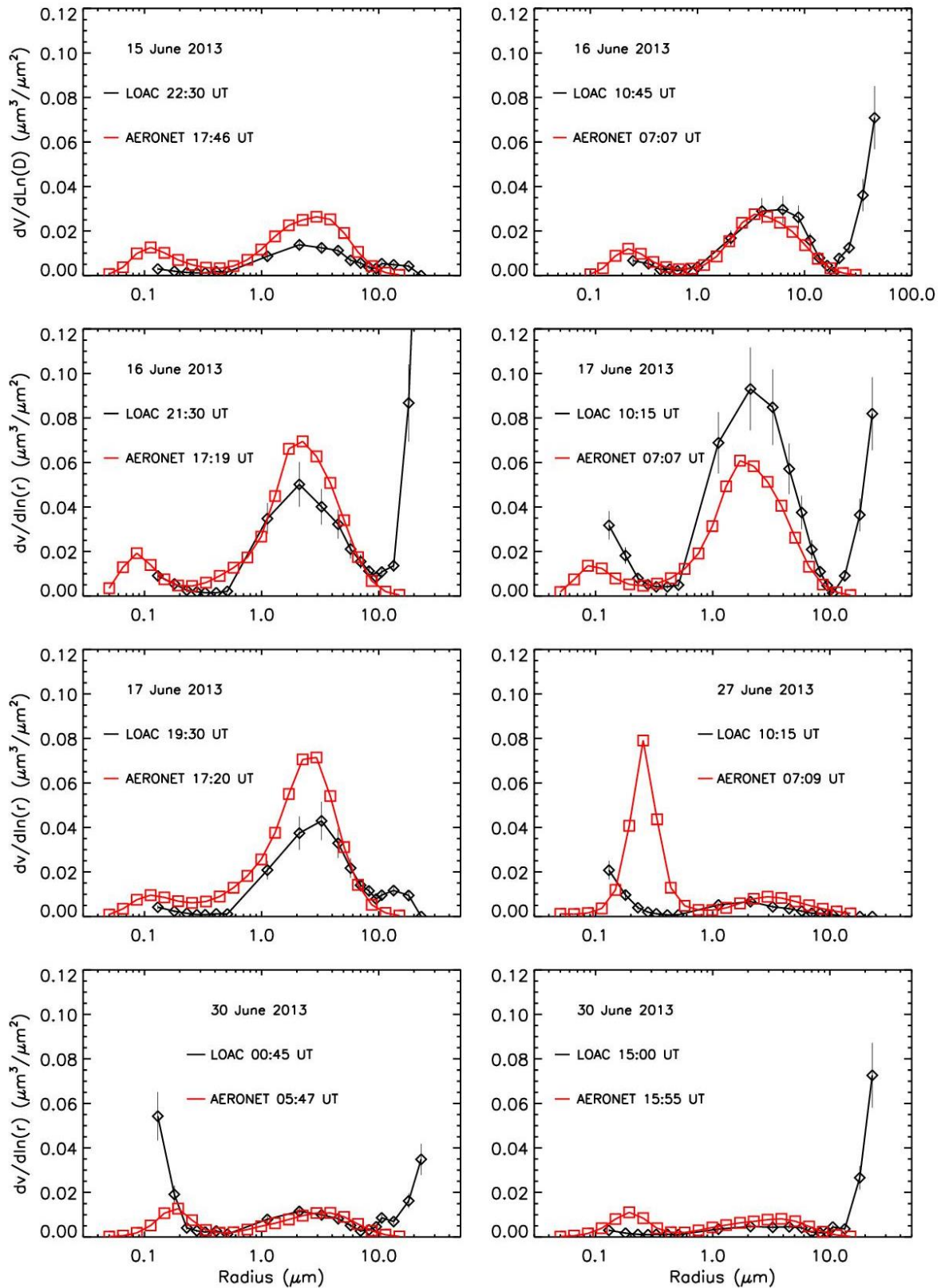
1036

1037 **Figure 12.** Comparison of the particle size distributions during the 16 June dust plume event over  
1038 Minorca, obtained with LOAC instruments under balloons and particle counters on board the ATR-42  
1039 aircraft; measurement altitudes are given.

1040

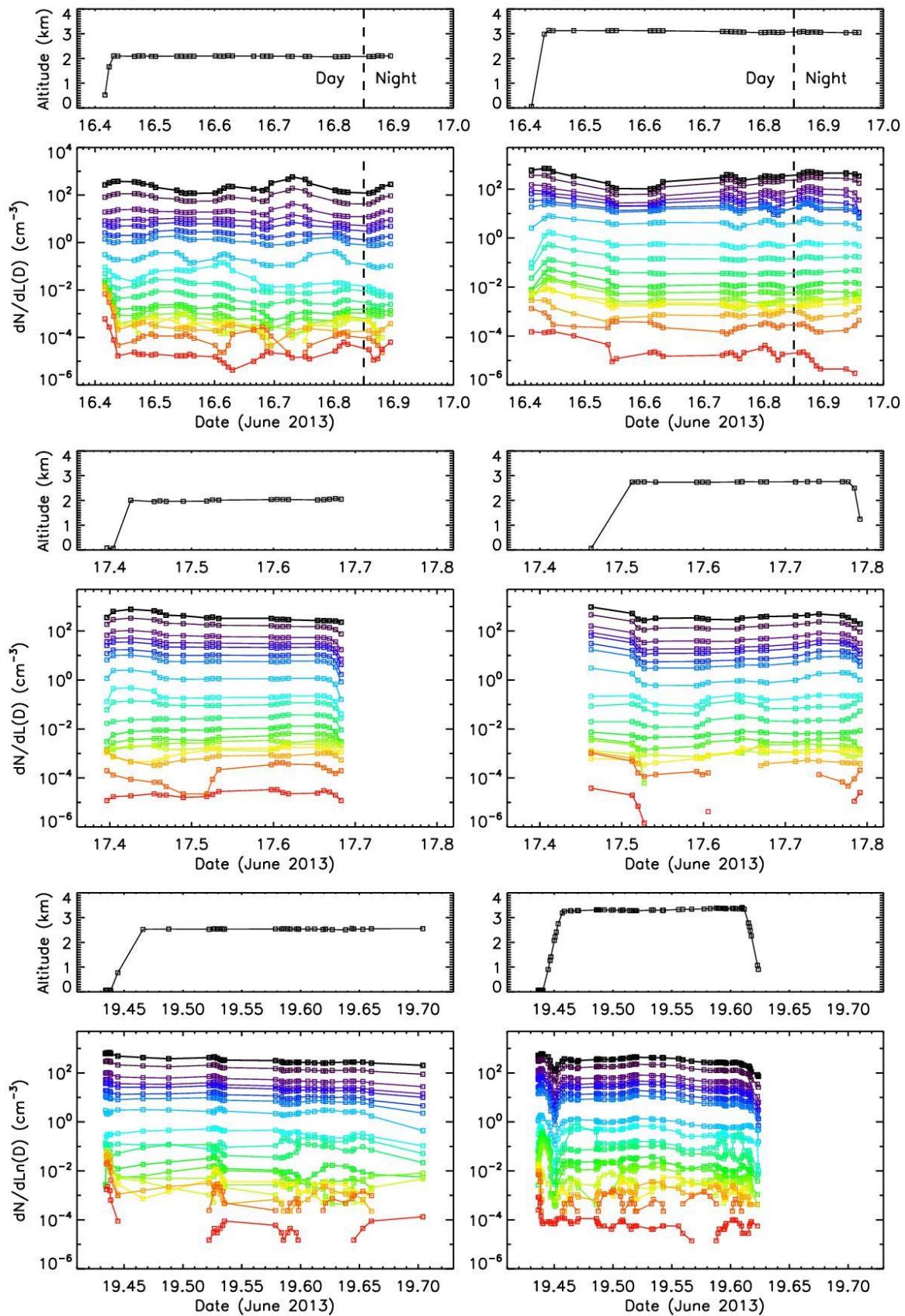
1041





1042  
 1043  
 1044  
 1045  
 1046

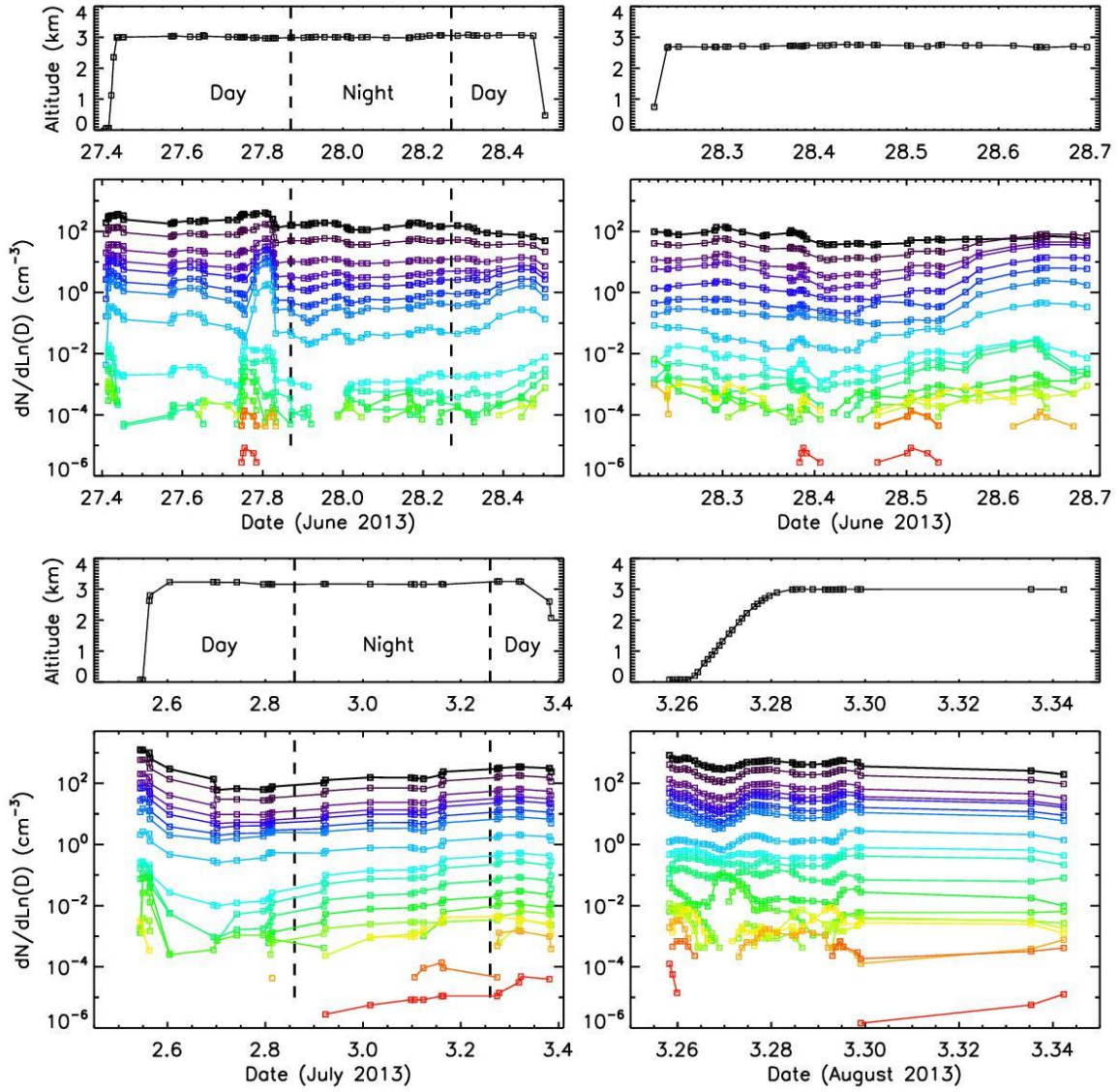
**Figure 13.** Volume size distribution retrieved from AERONET (<https://aeronet.gsfc.nasa.gov/>) and LOAC data on Minorca during the June 2013 plume events.



1047  
 1048  
 1049  
 1050  
 1051

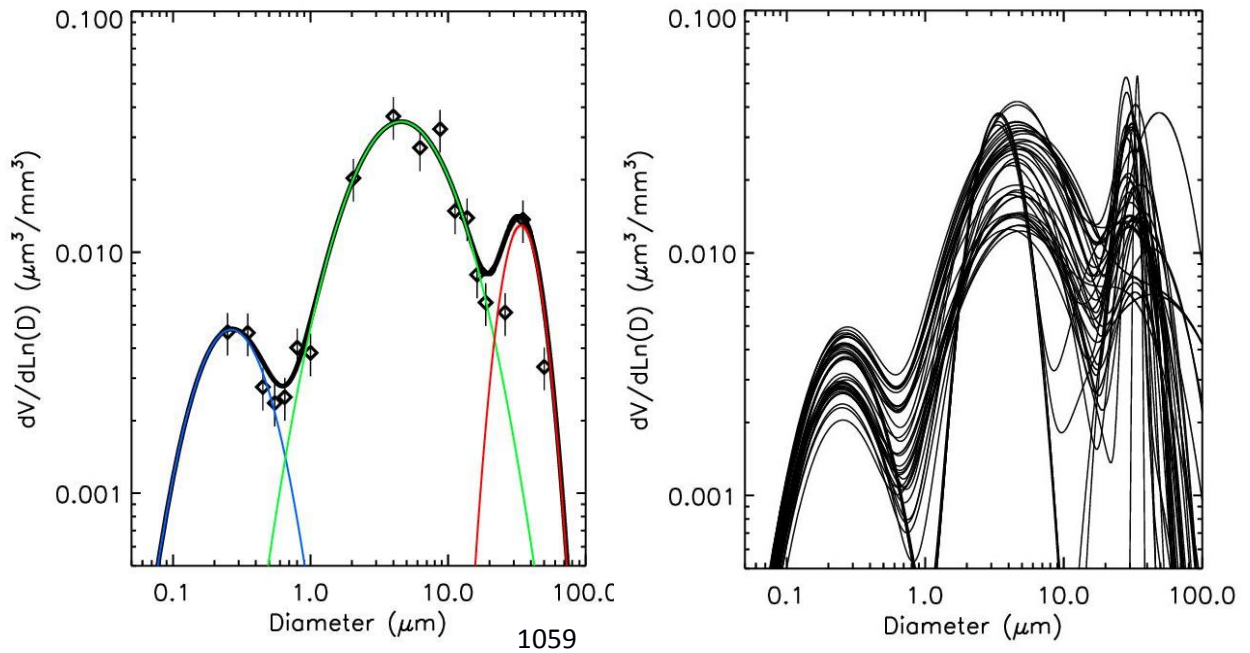
**Figure 14.** Each pair of graphs represents the time series of flight altitude (top) and LOAC-derived aerosol concentration for the 19 size classes (bottom), for BLPB flights from Minorca towards French coast. Colour coding is as in Fig. 7. Day-night transitions are indicated by dashed lines when appropriate.

1052



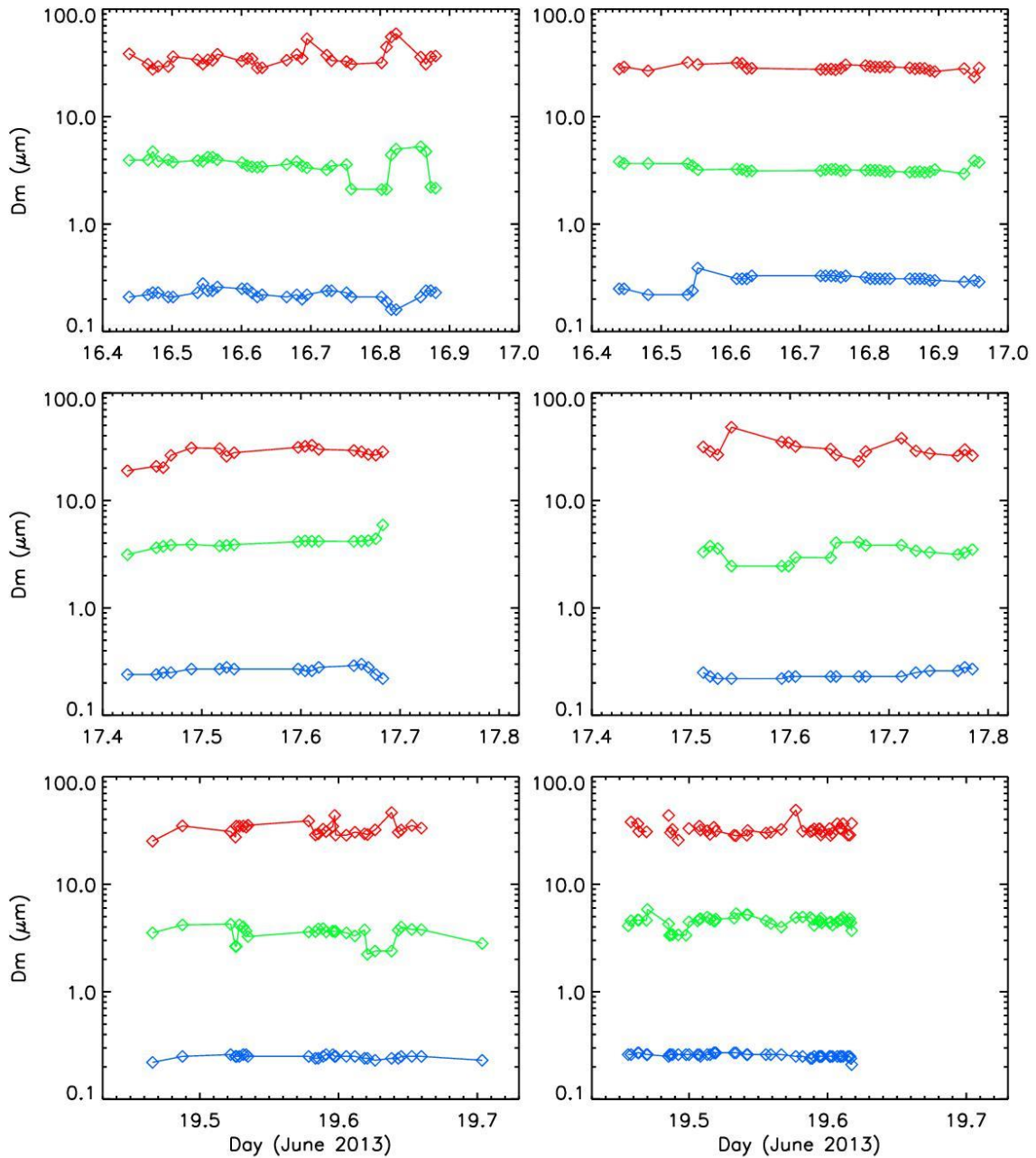
1053  
1054  
1055  
1056

Figure 14, continued.



1057  
 1058  
 1060  
 1061  
 1062  
 1063  
 1064  
 1065  
 1066  
 1067  
 1068

**Figure 15.** Left: Example of particle volume size distribution within the desert dust plume from the BLPB flight of 19 June 2013 at an altitude of 3.3 km, from one measurement at 12:30 UT. The black diamonds are the LOAC measurements (with 1- $\sigma$  error bars), the coloured curves represent the lognormal functions for each of the observed modes, and the black curve represents the overall fit (sum of the 3 modes). The geometric mean diameters ( $D_m$ ) of the 3 modes are of 0.27, 4.6 and 34  $\mu\text{m}$ , with respective geometric standard deviations ( $\sigma$ ) of 1.79, 2.14 and 1.35. Right: The 41 fitted size distributions when the third mode was detected, retrieved from all measurements during the 19 June BLPB flight at float altitude.

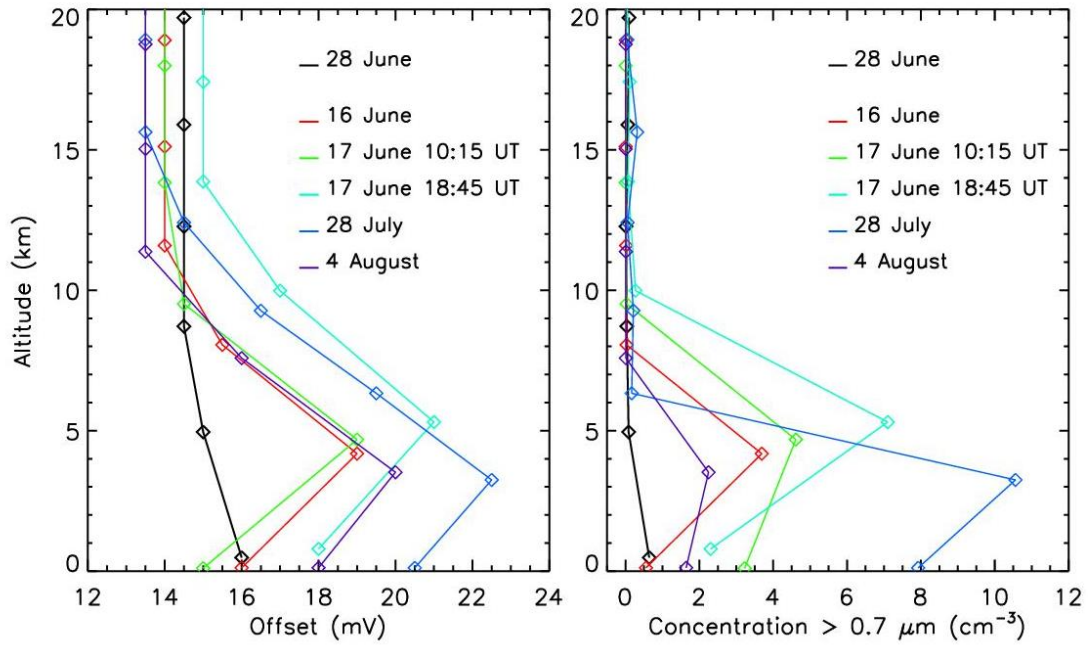


1069

1070

1071 **Figure 16.** Time-evolution of the particle size at the maximum concentration for each mode ( $D_m$ ) of  
 1072 the volume size distribution, at float altitude of BLPB flights from Minorca towards French coast. The  
 1073 altitudes are 2.1 and 3.1 km for the 16 June flights (top left and right, respectively), 2.0 and 2.7 km  
 1074 for the 17 June flights (middle left and right, resp.), and 2.5 and 3.3 km for the 19 June flights  
 1075 (bottom left and right, resp.). Average  $D_m$  values of the 3 modes during each flight are given in  
 1076 Table 3.

1077



1078  
 1079  
 1080  
 1081  
 1082  
 1083  
 1084

**Figure 17.** Left: Profiles of the LOAC electronic offset in case of crossing a strong dust plume (16 June, 17 June mid-time and evening, 28 July and 4 August) and in case of a weak dust plume just close to ground on 28 June. Right: Profiles of number concentrations of dust particles larger than 0.7 μm for the same flights.